water for life



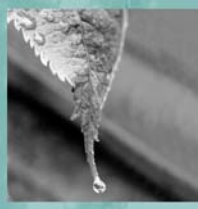

knowledge and research

Uranium and Arsenic Sources in Shallow Groundwater Near Bonnyville, Alberta: A Mineralogy Study

Alberta Innovates -Technology Futures, Alberta Environment and Water
Author: Moncur, M.C., Paktunc, D., Thibault, Y., Birks, S.J., Wieser, M.

March 2011

Government of Alberta

ISBN No. 978-0-7785-9615-8 (print version)
ISBN No. 978-0-7785-9616-5 (online version)

Disclaimer
The contents of this document have been prepared with funds from Alberta Environment and Water but do not necessarily reflect the Ministry's views or policies. Any mention of trade names or commercial products does not constitute an endorsement or recommendation for use.

Any comments, questions or suggestions on the content of this document may be directed to:

Alberta Environment and Water
Communications
7th Floor, Petroleum Plaza South Tower
9915-108 Street
Edmonton, AB T5K 2J6
Tel: 780-427-2700 (outside of Edmonton dial 310.0000 for toll-free connection)
Fax: 780-422-4086
E-mail: env.infocent@gov.ab.ca
Website: http://environment.gov.ab.ca/info/home.asp

Additional Copies
Additional print copies of this document are available from:

Alberta Environment and Water
Information Centre
4th Floor, Twin Atria Building
4999 – 98 Avenue
Edmonton, AB T5K 2J6
Tel: 780-427-2700 (outside of Edmonton dial 310.0000 for toll-free connection)
Fax: 780-422-4086
E-mail: env.infocent@gov.ab.ca
Website: www.gov.ab.ca/env

ISBN No. 978-0-7785-9615-8 (print version)
ISBN No. 978-0-7785-9616-5 (online version)

Uranium and Arsenic Sources in Shallow Groundwater Near Bonnyville, Alberta: A Mineralogy Study

Submitted By:
Michael Moncur, MSc.
Alberta Innovates – Technology Futures
3608 – 33 Street N.W.
Calgary, AB T2L 2A6
Tel. 403-210-5368
Michael.moncur@albertainnovates.ca

Contributors:
Michael Moncur[1], Dogan Paktunc[2], Yves Thibault[2], Jean Birks[1], Michael Wieser[3]
[1]Alberta Innovates – Technology Futures
[2]CANMET Mining and Mineral Sciences Laboratories, Ottawa, ON
[3]Dept. of Physics and Astronomy, University of Calgary, Calgary, AB

March 31, 2011

Funding for this research was provided by Lakeland Industry and Community Association (LICA), the Beaver River Watershed Alliance, and Alberta Environment and Water

INTRODUCTION

Elevated dissolved uranium (U) concentrations were measured in shallow aquifers at two locations within the Cold Lake - Beaver River Basin (Figure 1). In 2009 field investigations were conducted by Alberta Innovates-Technology Futures (AITF) at the two sites to determine if the sources of dissolved U concentrations to the groundwater were anthropogenic or natural (Moncur, 2010). The study did not find any indication that elevated dissolved U concentrations were the result of energy operations or agricultural practices. Total digestion analysis of the clay till material overlying the shallow aquifers revealed that the till contained solid-phase U concentrations up to 2.7 mg kg^{-1}, similar to the range reported in the area (3-5 ppm by weight,; Andriashek, 2000). Till at both sites show oxidation at depths to 5.8 m and 4.9 m at Site 1 and Site 2, respectively. This suggested that the primary source of U concentrations to groundwater in shallow aquifers may be from the weathering of overlying uranium-bearing tills which release dissolved concentrations of uranium to the adjacent pore waters.

In order to fully understand the source and release of uranium to the till pore water and underlying aquifers, a detailed mineralogical analysis of the sediments from the two sites near Bonnyville, Alberta was conducted. This mineralogical study included analyses of till, aquifer and secondary precipitate samples for identification of primary U minerals, chemical composition of the minerals, surficial features documenting the extent of weathering, and any secondary mineral phases. The mineralogical study involved the characterization 13 samples (nine from Site 1 and four from Site 2), with the purpose to determine the sources of uranium. Although dissolved arsenic (As) concentrations at Sites 1 and 2 did not exceed drinking water guidelines, elevated concentrations of this metal have been measured from groundwaters in other areas of the Beaver River Watershed (Alberta Health and Wellness, 2000; Lemay et al., 2005), therefore it was decided to also investigate As bearing mineral phases in the sediments during this study.

BACKGROUND

After deposition of glacial tills, weathering occurs as oxygen diffuses into the soils, resulting in the oxidation of minerals and the release of dissolved ions into the pore water. Over time, oxidized meteoric water eventually displaces the original pore water moving downward through the till deposits via pore space and fractures. Although clays tend to have a very low intergranular permeability, they are often fractured and have thin lenses of silt which may increase the permeability. Examples of this can be found in the glacial till deposits of central Saskatchewan (Ranville, et al., 2007), where weathering over the past 7 ka to 10 ka has resulted in oxidation of the tills to a depth of 4 m. The oxidized zone is characterized by a brown color and the presence of fractures. Oxidation of the till at that site resulted in the release of elevated concentrations of dissolved U and other ions to the pore water. The leaching of U and other metals from tills due to surficial weathering has also been observed in Southern Alberta (Ivanovich et al., 1991), southeastern Manitoba (Betcher et al., 1988), and Northern Ontario (Gilliss et al., 2004).

SITE DESCRIPTION

The study sites are located near Bonnyville, Alberta (Figure 2). Site 1 (3-15-061-05 W4M) and Site 2 (NE-22-063-05 W4M) are located approximately 22 km apart. The area lies within the Eastern Alberta Plains and Mostoos Hills Upland regional Physiographic units. Both study sites

are within the Eastern Alberta Plains and have an elevation typically below 600 m (Atlas of Alberta, 1969). The area is glaciated with relief ranging from flat to hummocky. The two sites lie within the Beaver Lowlands, a flat-to-gently-rolling till plain (Andriashek and Fenton, 1989). Sites 1 and 2 are both located in the Reita Lake Member (Pleistocene epoch) of the Grand Centre Formation. This diamicton till is composed of clayey-sand, rich in igneous and metamorphic rock fragments derived from the Canadian Shield (Andriashek, 2000).

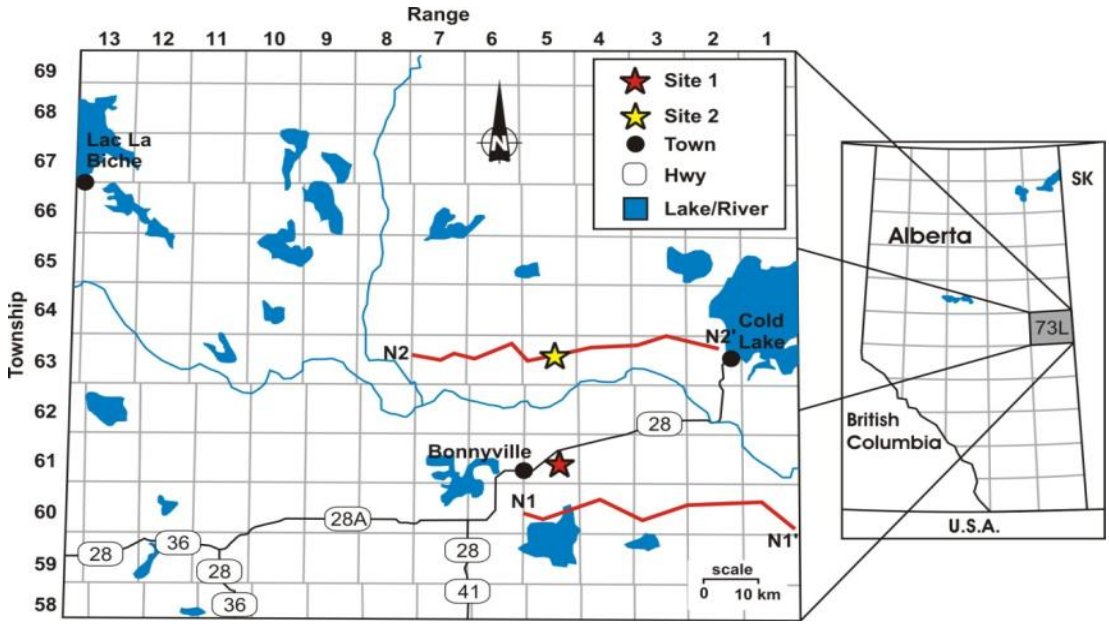

Figure 1: Map showing locations of Site 1 and Site 2.

The climate of the area is Dfb (long cool summers with severe winters), based on the Köppen classification. The mean annual precipitation in 433 mm and potential evapotranspiration is 508 mm per year (Hydrogeological Consultants Ltd., 2002).

Site 1

Site 1 is located approximately 2 km east of Bonnyville, Alberta (Figure 1). The property is flat in topography and bounded by highway 659 to the south, farm land to the north and east, and commercial property to the west. Approximately 300 m to the north of the site is an energy well battery. At the battery, crude oil is separated from impurities. Water produced from the separation process (processed water) is stored in tanks then periodically emptied into tanker trucks and hauled offsite. There are five water wells located at Site 1 over two residential properties (Figure 2). Three water wells are located on Resident A's property (Well 1, Well 2 and Well 3); and the adjacent property to the west has two water wells (Well 4 and Well 5). In 2009 AITF installed a bundle piezometer (MW1) near Well 1 and the monitoring piezometer (MW2) at a location that would not be influenced by the pumping of any existing wells (Figure 2). For additional information including a detailed description of well dimensions and depths see Moncur (2010). The groundwater beneath Site 1 flows from south to north (Hydrogeological Consultants Ltd. 2007), towards the energy well battery. Except for Well 5, groundwater from all other wells and piezometers at Site 1 contain elevated U concentrations exceeding the current Canadian Drinking Water Quality Limit of 20 µg L^{-1} (Table 1) (Health Canada, 2010).

Hydraulic head measurements from the piezometer nest at Site 1 indicate very little vertical hydraulic gradients.

Table 1: Site 1 water well depths with dissolved concentrations of uranium and arsenic measured in 2009. Concentrations in bold exceed the Canadian Drinking Water Standard of 20 and 10 µg L^{-1} for uranium and arsenic, respectively.

Location-Site 1	Depth (m)	Uranium (µg L^{-1})	Arsenic (µg L^{-1})
MW1-1	7.6	**23.4**	1.1
MW1-2	9.4	**21.4**	1.8
MW1-3	13.9	**27.7**	3.4
MW2	7.2	**81.6**	1.3
Well 1	6.9	**151**	2.0
Well 2	7.4 (12.2)	**75**	1.8
Well 3	21.5	**68.3**	1.8
Well 4	10.1	**26**	0.9
Well 5	24.8	4.5	0.8

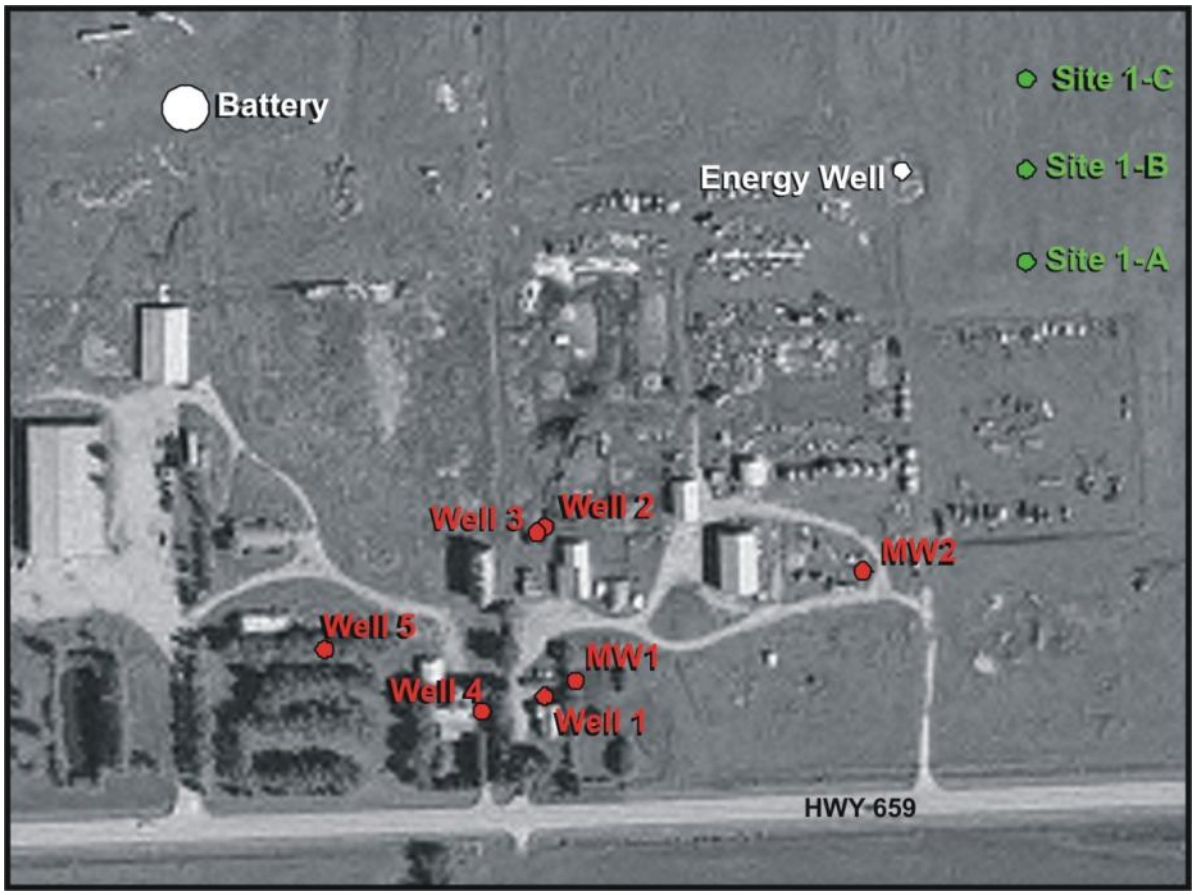

Figure 2: Aerial view of Site 1 showing the locations of water wells, monitoring wells, battery and energy well.

Site 2

Site 2 is located approximately 23 km NE of Bonnyville, Alberta (Figure 1). The property has hummocky-like terrain with the south portion in a topographic low, rising in elevation to the north of the property. The property is bounded by Range Road 452 to the west, a forested marsh area to the south and farmland to the north and east. The farmland is used for hay crops and cattle grazing. On the south portion of the property there are three wells of interest (Well 1, Well 2 and Well 3). The wells are located near a pond of standing water that collects surface water drainage from the surrounding area. Well 1 and 2 are located adjacent to a cattle feedlot. In 2009 AITF installed two monitoring wells at Site 2; a bundle piezometer and a background monitoring piezometer (Figure 3). The bundle piezometer (MW1) was installed 8 m from Well 1 and the monitoring piezometer (MW2) was installed 172 m NE of Well 1 to prevent any influences from the pumping of existing wells. Hydraulic head measurements from the piezometer nest at Site 2 show a very strong vertical hydraulic gradient indicating downward flow of groundwater. Approximately 280 m north and up-gradient of Well 1 is an energy well battery. Also up-gradient 125 m NW of Well 1 is a field where fertilizer was previously applied. Assuming that groundwater follows the local topography, groundwater in the area would flow from north to south. Sampling conducted by Moncur, 2010, show that the groundwater from monitoring wells MW1, 2, and 3, and water wells 1 and 3, contain elevated U concentrations exceeding the current Canadian Drinking Water Quality Limits of 20 µg/L.

Table 2: Site 2 water well depths with dissolved concentrations of uranium and arsenic measured in 2009. Concentrations in bold exceed the Canadian Drinking Water Standard of 20 and 10 µg L^{-1} for uranium and arsenic, respectively.

Location-Site 2	Depth (m)	Uranium (µg L^{-1})	Arsenic (µg L^{-1})
MW1-1	1.6	10.2	8.7
MW1-2	3.8	**40.5**	5.4
MW1-3	12.5	**25.8**	4.3
MW2	10.7	1.8	**12.2**
Well 1	12.3	**29.3**	1.0
Well 2	20.2	13.7	0.9
Well 3	26.8	**22.3**	1.0

Figure 3: Aerial view of Site 2 showing the locations of water wells, monitoring wells and battery.

METHODS

During drilling at Sites 1 and 2 in November 2009, sediment samples were collected using a split spoon or sampled from the auger. Samples were collected every 0.25 m over the first 3 m of drilling followed by sampling at 0.5 m intervals for the remaining depths. Samples were placed in sealable freezer bags and immediately frozen after collection due to the subzero outside temperature. All samples were transferred to a freezer at AITF in Calgary. Selected samples were spilt into four subsets to conduct whole rock analysis, detailed mineralogy, pore water extraction and moisture content. Any remaining sample was archived.

Whole Rock Analysis and Gravimetric Moisture Content

Depth profiles of sediment whole rock analysis were measured at Sites 1 and 2, presented in Moncur (2010). For this study, 4 additional sediment samples were analyzed and added to the depth profiles. Sediments include two samples from Site 1 from depths of 10.7 and 14 m, and two samples from Site 2, from depths of 8 and 13.5 m. Samples were microwave digested in 5 mL nitric acid, 2 mL hydrogen peroxide and 1.5 mL hydrofluoric acid. Following total

digestion, samples were diluted and total concentrations of U, Iron (Fe), Aluminum (Al), As, Calcium (Ca), Magnesium (Mg), Sodium (Na), and Potassium (K) were measured using inductively coupled plasma atomic emission spectroscopy (ICP-MS) at the AITF laboratory in Vegreville, Alberta.

Gravimetric moisture content was measured on 19 sediment samples from Site 1 and 21 samples from Site 2. Sediment samples were weighed, dried in an oven at 105 ^{0}C for 24 hours, and then reweighed.

Mineralogy

The samples for mineralogical analysis were shipped frozen to CANMET Mining and Mineral Sciences Laboratories in Ottawa, ON. Thirteen samples were analyzed from Site 1 (seven sediment and two secondary precipitates) and 4 sediment samples from Site 2. Frozen samples were air-dried, de-agglomerated, homogenized and split into representative fractions. Primary crystalline phases were determined for all samples by X-ray Diffraction (XRD) using a RIGAKU D/MAX 2500 rotating-anode powder diffractometer. More detailed identification of individual phases in the secondary precipitates was made using a Rigaku Rapid II rotating anode micro-XRD. For some samples, mineral species identified by XRD were confirmed by energy – dispersive spectrometry (EDS) using a JEOL JXA 8900 electron probe micro-analyzer (EPMA) to provide qualitative information about the composition of the main mineral phases observed in the polished section. Backscattered electron imaging (BSE) and quantitative wavelength-dispersive X-ray spectrometry (WDS) were used to locate and determine quantitatively the compositions of the main carriers of U and As.

X-ray absorption fine spectroscopy (XAFS) experiments were carried out at the bending magnet beamline of the Advanced Photon Source (APS), Argonne, Illinois, USA. The XAFS was used to determine the valence states to U and As mineral phases. Finely ground and homogenized samples were loaded into Teflon sample holders with Mylar windows. Experiments were carried out at room temperature in the fluorescence mode using a Canberra 13-element detector. A gold foil was used for energy calibration for As K-edge and a Zirconium foil for the U L(III)-edge XAFS measurements. Between five to eight scans were made on each sample. Data reduction and analysis were performed with ATHENA (Ravel and Newville, 2005). The least-squares fitting analyses of the X-ray absorption near edge structure (XANES) spectra were performed with LSFitXAFS (Paktunc, 2004).

Pore Water Extraction and Analysis

Sediment samples for pore water extraction were thawed overnight in a refrigerator at 4^{0}C. To separate pore water from sediments, samples were transferred to Nalgene 50 mL Oak Ridge centrifuge tubes. Sample tubes were rotated for two hours at 10,000 rpm at a constant temperature of 4 ^{0}C using a Sorvall RC-6 Plus Superspeed Centrifuge. Elevating temperatures above ambient field temperatures during centrifuging has been shown to increase concentrations of silica and pH in pore water (Fanning and Pilson, 1973). Separated pore water was carefully decanted from the sediments using a pipette and transferred to 8 mL Nalgene bottles. The pore water was again centrifuged at 10,000 rpm for 30 minutes to separate any suspended solids. Pore water was carefully decanted from the bottles with a pipette, passed through a 0.45 μm filter. Where sample volume was sufficient, the filtered sample was split into three aliquots: anions, cations (preserved with 12 *N* trace-metal grade HNO_3 to a pH of <1), and

pH and alkalinity. Pore water was separated from a total of 24 clay samples; 10 from Site 1 and 14 from Site 2.

Pore water pH was measured from each sample immediately after centrifuging using an Accumet electrode (model 13-620-290) calibrated with standard buffer solutions at pH 7, 4, and 10. Samples were then measured for alkalinity using a Hach digital titrator and bromcresol green/methyl red indicator and with 0.16 *N* Sulfuric acid (H_2SO_4). All samples for cations and anions were immediately refrigerated until analysis. Samples were shipped to the University of Waterloo and analyzed using ICP-OES for major cations, ICP-MS for trace metals and ion chromatography (IC) for anions. $^{234}U/^{238}U$ activity ratios were measured using multi collector inductively coupled plasma mass spectrometry (MC-ICP-MS) (McKiernan, 2011).

Geochemical Modeling

The geochemical model PHREEQC 2.15.0 (Parkhurst and Appelo, 1999) using the WATEQ4F (Ball and Nordstrom, 1991) database was used to understand secondary mineral phases that may be controlling dissolved uranium and arsenic concentrations in groundwater and pore water sampled from Site 1 and Site 2. PHREEQC is an equilibrium/mass-transfer model that calculates saturation indices (SI) for discrete mineral phases. An SI value greater than zero suggests that the water is supersaturated with respect to the mineral phase and may precipitate; an SI value less than zero suggests that the water is undersaturated with respect to the mineral phase will not precipitate; and an SI value near zero indicates that the water is at equilibrium with respect to the mineral phase. The WATEQ4F thermodynamic database contains dissolved U species and U minerals. The PHREEQC allows oxidation–reduction potentials (ORP) be entered as measured pe. Eh was not measured from the pore water samples therefore Eh was estimated from measured values in adjacent sand units.

RESULTS AND DISCUSSION

Stratigraphy and Sediment Mineralogy

The stratigraphy at Site 1, includes brown oxidized clay to a depth of 5.8 m overlying unoxidized grey stiff clay with sand lenses (Figure 4). The oxidized clay contained some silt lenses, pebbles and the occasional boulder. Within the upper meter, vugs contained a white powdery mineral interpreted to be gypsum, as has been observed in similar tills (Hendry et al., 1986). Below 1 m, vugs with red iron-like minerals and iron staining along possible fractures were observed to a depth of 5 m. At a depth of 5.8 m, there was a sharp transition from brown oxidized clay to grey stiff clay. A brown fine-to-medium-grained water-bearing sand was present from 6.4 to 6.7 m followed by grey clay. A second water-bearing unit composed of a medium to coarse-grained grey sand was observed from 9.15 to 9.76 m. Dense grey clay extended from 9.76 m to 12.2 m at which point a third water–bearing unit, consisting of a grey silty-sand was observed from 12.2 to 13.7 m. Grey clay was encountered from 13.7 to 15.2 m. A fourth saturated sand unit was located at a 22 m depth.

Sediment stratigraphy from Site 2 revealed brown oxidized clay-till to a depth of 4.9 m overlying a grey pebbly clay till with sand lenses (Figure 5). The brown oxidized clay contained silt lenses and pebbles. A brown saturated silt layer was observed between 1.5 m and 1.75 m, and a water-bearing unit consisting of brown saturated sandy-silt was encountered between 3 and 3.5 m. At a depth of 4.9 m, there was a transition from brown oxidized clay to grey pebbly

clay. A grey fine to medium grained water-bearing sand was encountered from 12 to 12.3 m followed by grey clay. Grey clay was encountered from 12.3 to 13.5 m. Deeper saturated sand units were present at depths of 21 m and 26.8 m.

The results of the XRD analyses revealed similar mineralogical compositions in the sediments from Sites 1 and 2, with the crystalline phases consisting mainly of quartz (SiO_2) microcline ($KAlSi_3O_8$), albite ($NaAlSi_3O_8$), calcic plagioclase ($CaAl_2Si_2O_8$) calcite ($CaCO_3$), amphibole with various amounts of clays minerals (kaolinite ($Al_2Si_2O_5(OH)_4$) and/or montmorillonite [$(Na,Ca)_{0,3}(Al,Mg)_2Si_4O_{10}(OH)_2 \cdot n(H_2O)$]) and mica (phlogopite) [$K(Mg,Fe)_3(Si_3Al)O_{10}(OH)_2$] or muscovite [$KAl_2(AlSi_3O_{10})(OH)_2$]). No obvious mineralogical differences were observed between the oxidized and unoxidized till units. The main mineralogical difference between the till and sand sediments was found to be a higher proportion of dolomite ($CaMg(CO_3)_2$) and clay minerals in the clay-till, as reflected in the bulk chemical compositions (Figures 4 and 5). The higher proportion of dolomite and clay minerals in the tills are likely responsible for the higher solid-phase concentrations of Ca, Mg and Al in the tills than in the water-bearing sand units.

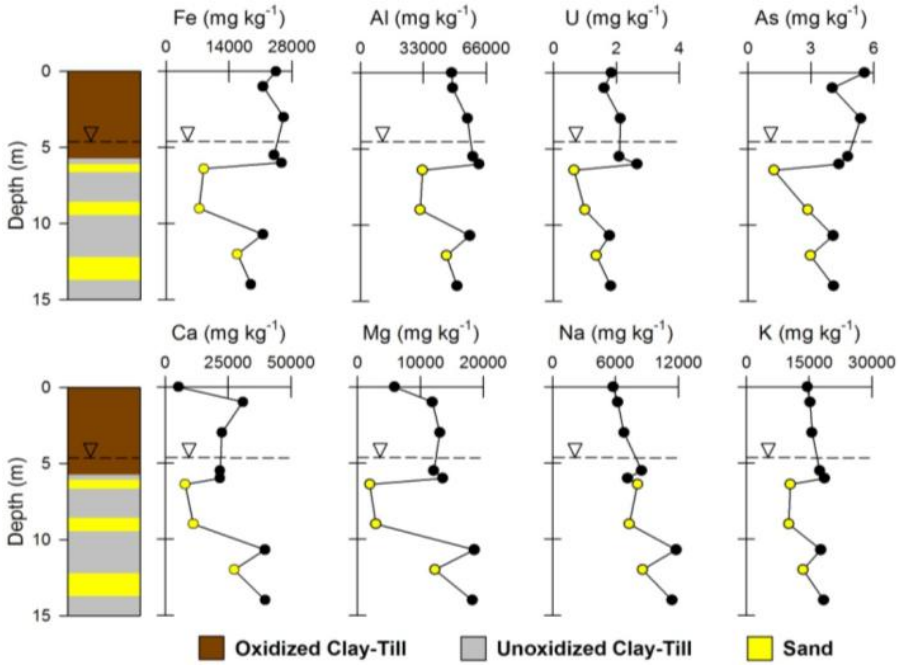

Figure 4: Depth profile showing stratigraphy and total solid concentrations at Site 1, MW1. The dashed line with inverted triangle represents the water table. Yellow data points indicate sediment sampled from the sand units, black data points are from the till.

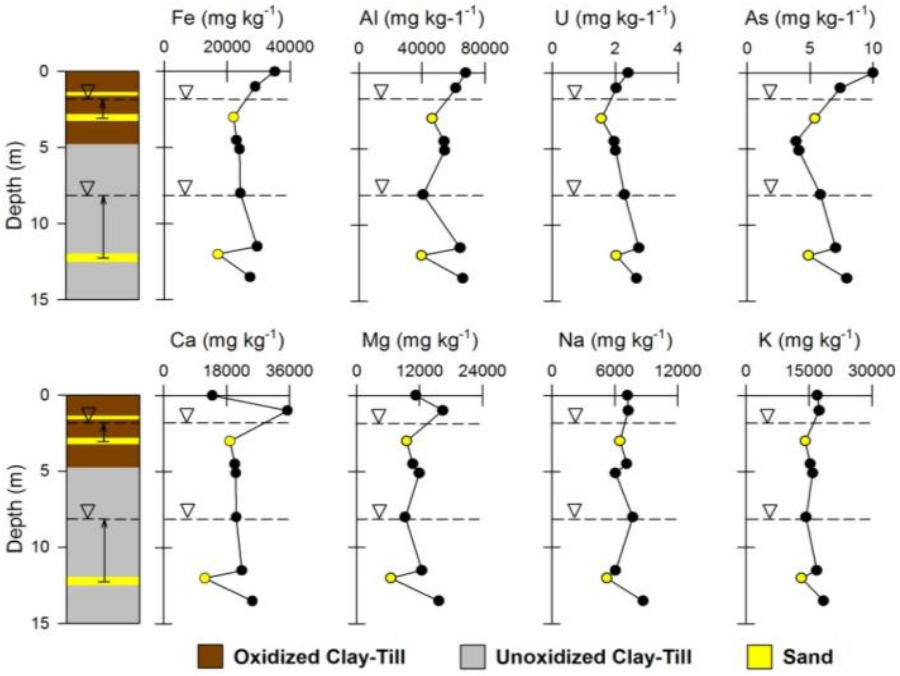

Figure 5: Depth profile showing stratigraphy and total solid concentrations at Site 2, MW1. The dashed line with inverted triangle represents the water table for the upper and lower aquifers. Yellow data points indicate sediment sampled from the sand units, black data points are from the till.

Despite similarity in mineralogical composition, there are notable differences in the depth profiles of total solid concentrations for the major cations and metals at Site 1 well, MW1 (Figure 4) and Site 2, MW1 (Figure 5). At Site 1, solid concentrations of major cations, Al and U are lower in the in the near-surface oxidized sediments and these ion concentrations increase with depth toward the unweathered clay-till material (Figure 4). This is consistent with the upper portion of the profile representing a zone of leaching due to the greater exposure to weathering (White, 2003). In this zone, concentrations of major cations, Al and U are depleted due to mobilization through weathering processes and displaced downwards by meteoric water. With depth, the ingress of oxygen decreases resulting in an underlying, unoxidized zone where the solid phase concentrations of total metals and major cations remain high. Concentrations of major cations and metals are generally lower within the aquifer materials then the adjacent clay units. This pattern of lower solid phase concentrations in the oxidized zone is not present at Site 2. At this site solid phase concentrations of Fe, Al, and As are highest in the immediate near surface sample. As with Site 1 the sand units contained the lowest concentrations of solid phase concentrations.

Groundwater and Pore Water Chemistry

There are differences in the distribution of major cations and trace metals at the two sites (Figure 6 and 7) likely related to differences in the degree of weathering and hydrogeological setting of the two sites, and the proximity of Site 1 to a fertilized garden.

At Site 1, concentration of Sulphate (SO_4), dissolved major cations, and trace metals are elevated in the near surface of the weathered till with maximum concentrations of 2713 mg/L SO_4; 993 mg/L Ca; 1005 mg/L Na; 1010 mg/L Mg; 24 mg/L K; and 2.1 mg/L Sr. Dissolved

concentrations of ions decrease by an order of magnitude with depth towards the water table and into the unweathered till. The elevated concentrations of dissolved ions at shallow depths in the profile at Site 1 is consistent with what has been observed in tills in southern Saskatchewan and Alberta where chemical weathering since deglaciation has resulted in elevated concentrations of weathering products in the oxidized zone (Hendry et al., 1986; Hendry and Wassenaar, 2000; Yan at al., 2001).

Pore water collected from the weathered clay/till at Site 2 does not contain elevated concentrations of dissolved ions such as the weathered zone at Site 1 (Figure 7).

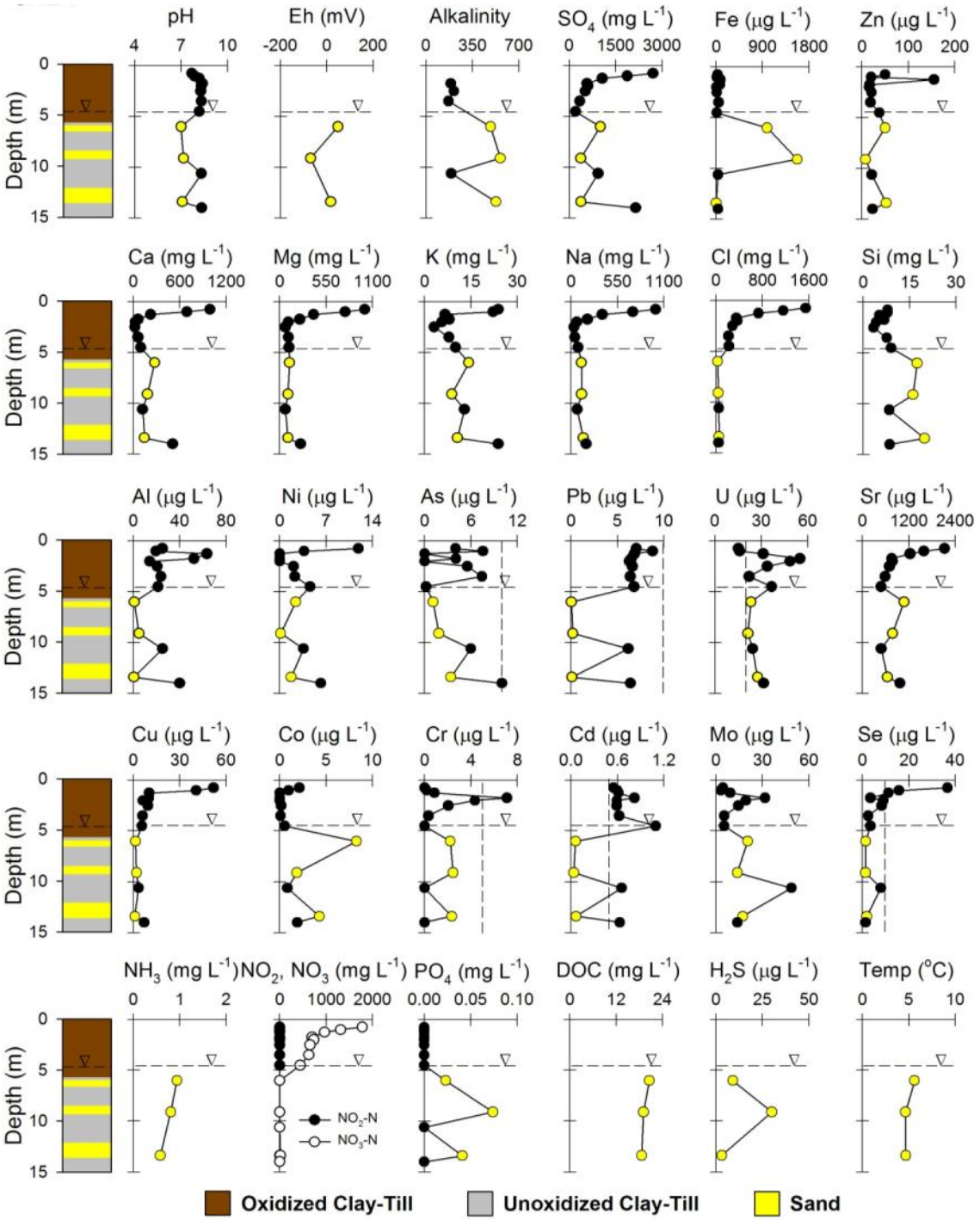

Figure 6: Depth profile showing stratigraphy and dissolved solutes from Site 1 at location MW1. The dashed line with inverted triangle represents the water table. Yellow data points represent samples from piezometers, black symbols represent pore water obtained by centrifuging.

Chemical weathering and subsequent dissolution of minerals such as calcite and dolomite release concentrations of Ca, Mg and bicarbonate (HCO_3) to the pore water (Langmuir, 1997) through the following equations:

$CaCO_3 + CO_2 + H_2O \leftrightarrow Ca^{2+} + 2HCO_3^{2-}$ (Equation 1)
Calcite

$CaMg(CO_3)_2 + CO_2 + H_2O \leftrightarrow Ca^{2+} + Mg^{2+} + 2HCO_3^{2-}$ (Equation 2)
Dolomite

The elevated concentrations of Ca and Mg in the weathered till at Site 1 (Figure 6) are likely a result of dissolution of calcite and dolomite according to equations 1 and 2, respectively. Solid phase concentrations of Ca and Mg in the upper till/clay are significantly depleted in the near surface zone of the weathered till indicating that leaching of Ca and Mg bearing minerals has occurred (Figure 4). Strontium is a common component of carbonate minerals and shows a similar trend in dissolved concentrations as dissolved Ca and Mg concentrations, suggesting Sr increases are related to carbonate dissolution. Near surface weathering may also promote weathering and hydrolysis of aluminosilicate minerals and release of dissolved ions to the pore waters (Langmuir, 1997):

$2KAlS_3O_8 + 2CO_2 + 11H_2O \rightarrow 2K^+ Al_2Si_2O_5(OH)_4 + 2HCO_3^-$ (Equation 3)
Microcline *Kaolinite*

$2NaAlSi_3O_8 + CO_2 + 11H_2O \rightarrow 2Na^+ + Al_2Si_2O_5(OH)_4 + 4H_4SiO_2 + 2HCO_3^{2-}$ (Equation 4)
Albite *Kaolinite*

Dissolution of microcline and albite feldspars, for example, as shown in equations 3 and 4, results in the release of dissolved K, Na and HCO_3 to the pore waters and hydrolysis of the Al-silicate minerals forming kaolinite. During mineralogical analysis kaolinite was identified within the weathered zone of the till. Gypsum observed in the weathered clay may also contribute to elevated pore water concentrations through dissolution, releasing Ca and SO_4 through equation 5:

$CaSO_4 \cdot 2H_2O \leftrightarrow Ca^{2+} + SO_4^{2-} + 2H_2O$ (Equation 5)
Gypsum

In addition to chemical weathering, the oxidation of pyrite in the weathered clay will release dissolved sulfate, acid (H^+) and precipitate Fe-oxyhydroxides:

$FeS_2 + 15/4O_2 + 7/2H_2O \rightarrow Fe(OH)_3 + 2SO_4^{2-} + 4H^+$ (Equation 6)
Pyrite

Mineralogy results from the weathered till at both sites revealed the presence of Fe-hydroxide pseudomorphs after pyrite, indicating that weathering of pyrite, according to equation 6, is likely occurring. The near-surface pore water pH is also slightly depleted with respect to pH values in the till with depth (Figure 6). Speciation modeling suggests that the pore water is saturated or supersaturated with respect to Fe-hydroxide which may account for the low concentration of dissolved Fe in the pore water of the weathered zone. The release of acid in equation 6 leads to the dissolution of carbonate and to some extent aluminosilicate minerals thereby increasing Ca, Mg and other ions in the pore water. For example the buffering of calcite and dolomite (Langmuir, 1997), and the hydrolysis of albite (White, 2003) and phlogopite

(Banfield and Eggelton, 1988; Malmström et al., 1996; Murakami et al., 2003) will consume acid, releasing Ca, Mg, Na and K to the pore water, as:

$CaCO_3 + H^+ \leftrightarrow Ca^{2+} + HCO_3^{2-}$ (Equation 7)
Calcite

$CaMg(CO_3)_2 + 2H^+ \leftrightarrow Ca^{2+} + Mg^{2+} + 2HCO_3^{2-}$ (Equation 8)
Dolomite

$2NaAlSi_3O_8 + 2H^+ + H_2O \rightarrow 2Na^+ + Al_2Si_2O_5(OH)_4 + 4SiO_2$ (Equation 9)
Albite *Kaolinite*

$K(Mg_2Fe)(AlSi_3)O_{10}(OH)_2 + 5H^+ + 0.25O_2 + 3H_2O \rightarrow K^+ + 2Mg^{2+}$ (Equation 10)
Phlogopite $+ 0.5Al_2Si_2O_5(OH)_4 + Fe(OH)_3 + 2H_4SiO_4$

Elevated concentrations of dissolved trace metals (Figures 6) in the weathered till at Site 1 are likely the result of their release from the structure of carbonate and Al-silicate minerals during weathering. Using microprobe analysis, Moncur et al. (2005) measured Chromium (Cr) concentrations in garnet, phlogopite and amphibole in rock derived from the Canadian Shield in Manitoba. They concluded that partial dissolution of these minerals led to elevated dissolved Cr concentrations in the pore water.

The distribution of dissolved ions in the vertical profiles measured at Site 1 is likely due to a combination of transport of ions released during weathering of minerals present in the oxidized zone since deglaciation, and the more recent influence of fertilizer applied to the adjacent field. At Site 1, well MW1 was installed near the edge of a garden that has received an annual application of manure-fertilizer for over 90 years. The use of fertilizer can result in elevated concentrations of ions present in the fertilizer itself, but can also result in the enhanced dissolution of aquifer material. Nitrification of reduced Nitrogen (N) from manure-fertilizers in soils containing naturally occurring carbonate minerals, such as calcite and dolomite, can result in elevated Ca, Mg and Nitrate (NO_3) concentrations in groundwater (Böhlke, 2002):

$CaMg(CO_3)_2 + NH4^+ + 2O_2 \leftrightarrow Ca^{2+} + Mg^{2+} + NO_3^- + 2HCO_3^{2-} + H_2O$ (Equation 11)
Dolomite

Dissolved NO_3 concentrations are extremely elevated at a depth of 0.75 m (1783 mg/L NO_3-N) and decrease to 441 mg/L at a 4.5 m depth near the water table. Dissolved Chlorine (Cl) concentrations typically associated with the fertilizers (Núnez-Delgado, 2002) are also elevated near surface (1545 mg/L) and decrease to 223 near the water table. The average concentration of NO_3 and Cl below a depth of 7.6 m is 4.5 mg/L and 41 mg/L, respectively. Provided that dissolved NO_3 and Cl concentrations are a result of fertilizer application, and Cl behaves conservatively, the vertical travel time of pore water through the weathered clay is approximately 4.5 m over the past nine decades (~5 cm/yr). Although glacial clay and till deposits have low hydraulic conductivities and the vertical flow of solutes can be limited, in some conditions, small groundwater velocities have been measured in clay and till deposits (Desaulniers & Cherry 1989; Hendry & Wassenaar 1999). Fractures in glacial clay and till can influence the movement of solutes by increasing the distances travelled from tens of meters to

hundreds of meters, depending on the length and connectivity of the fractures (Desaulniers et al. 1982; McKay et al. 1993).

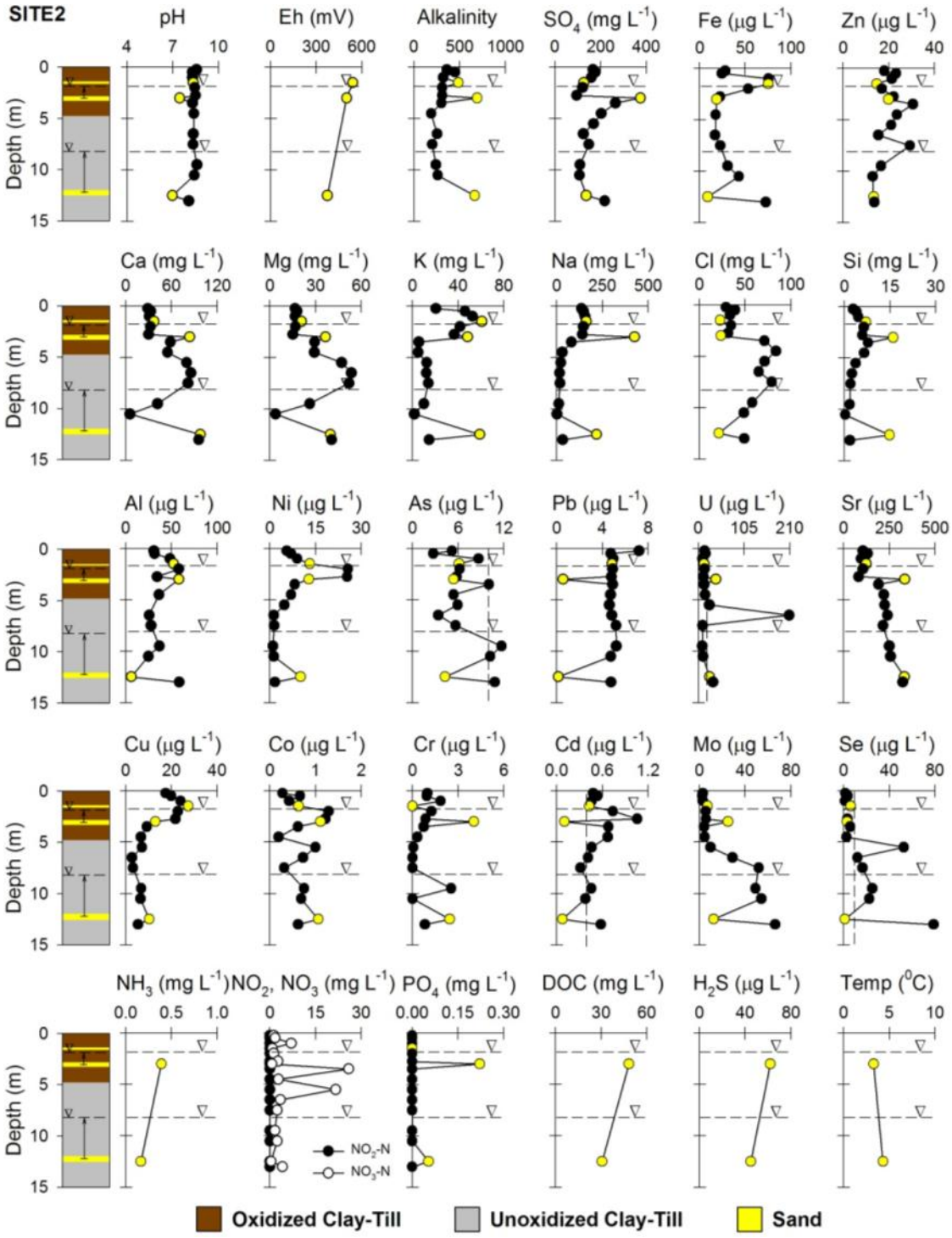

Figure 7: Depth profile showing stratigraphy and dissolved solutes from Site 2 at location MW1. The dashed line with inverted triangle represents the water table. Yellow data points represent samples from piezometers, black symbols represent porewater obtained by squeezing.

Pore water collected from the weathered clay-till at Site 2 does not contain elevated concentrations of dissolved ions such as the weathered zone at Site 1 (Figure 7). Although Sites 1 and 2 are mineralogically similar, concentrations of dissolved ions at Site 2 remain relatively constant through the weathered zone. This is likely due to higher water content in the sediments at Site 2 limiting weathering and oxidation processes (Figure 8). At Site 1, water content in the surface of the weathered clay is 1.7% increasing to 10 % at 2.5 m, whereas water content in the weathered clay surface at Site 2 is 6.7% increasing to 14% by 0.5 m.

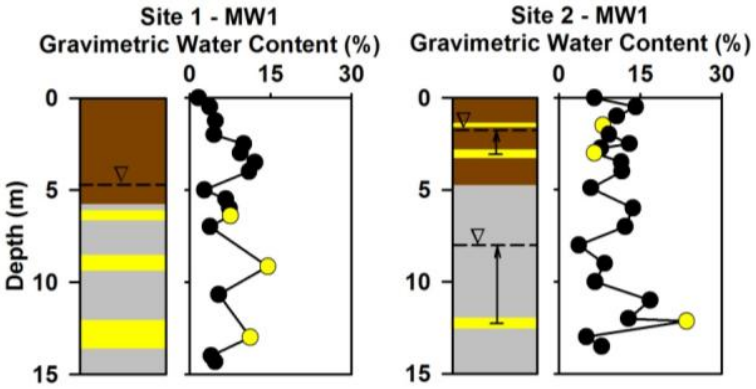

Figure 8. Depth profiles at Sites 1 and 2 showing stratigraphy and gravimetric moisture content of the sediments. The dashed line, with an inverted triangle above, represents the water table. Yellow data points represent samples from sand units and black symbols represent clay-till samples.

Uranium and Arsenic

The concentrations of U in the sediments range from 0.65 to 2.75 ppm (Figures 4 and 5), which is at the lower limits of where WDS-EPMA can be used. Because the concentrations of U were so low, and the mineralogy appeared to be fairly uniform, only four samples were analyzed using WDS-EPMA to characterize the mineralogy of the U and As carriers. These samples included one unweathered and one oxidized clay/till sample from each site. The samples were selected based on their U content:

- unweathered zone samples, S1-6 (U= 2.66 ppm, As= 4.34 ppm) and S2-11.5 (U= 2.75 ppm, As= 7.41 ppm),
- oxidized zone samples, S1-1 (U= 1.61 ppm, As=4.03 ppm) and S2-1 (U=2.03 ppm, As=7.41 ppm).

Uranium

Dissolved U concentration collected from pore water and groundwater at Site 1, MW1, show peak values in the weathered clay and relatively uniform values in the sand and unweathered clay units. Uranium pore water concentrations in the weathered clay averaged 32 µg/L and peaked to 55 µg/L at a depth of 1.75 m (Figure 6). All three saturated sand units contained dissolved U exceeding 20 µg/L, with an average of 24 µg/L (Table 1). Two pore water samples collected from the unweathered clay had an average concentration of 28 µg/L.

Pore water collected from the weathered zone at Site 2, MW1 contained dissolved U below 20 µg/L with an average concentration of 14 µg/L, however, a saturated silty-sand layer within this zone, at a 3 m depth, contains 41 µg/L of U (Figure 8). Pore water within the unweathered

clay remains below 20 µg/L until a depth of 5.5 m where the dissolved concentration of U increased to 25 µg/L then abruptly spiked to 208 µg/L at a depth of 6.5 m. The 6.5 m sample was supported by a duplicate analysis yielding a similar high concentration. As no other anomalous peaks of dissolved ions were observed, it appears that the sample was not contaminated. Therefore, the elevated concentration of dissolved U at 6.5 m is likely due to heterogeneities of U-bearing minerals in the adjacent sediments. The average concentration of dissolved U in the unweathered clay is 50 µg/L. The sand aquifer at 12.5 m contains a dissolved U concentration of 26 µg/L.

Solid phase U concentrations show an abrupt decrease in the aquifer material at Site 1 indicating that the coarser material contains a lower abundance of U than the clay/till material (Figure 4). Although the average concentration of solid-phase U in the clay-till material is quite low, similar U concentrations in Lake Agassiz clays (average 2.3 mg/kg) led to U concentrations in the till pore water up to 250 µg/L and in the underlying sand and gravel aquifers up to 155 µg/L (Betcher et al., 1988). The lower abundance of U in the actual sand aquifer sediments combined with the elevated concentrations of dissolved U, Na, Mg and SO_4 in groundwater in the shallow, uppermost aquifer at Sites 1 and 2 provides a strong indication that some elevated U concentrations are due to downward leakage of weathering products from the overlying clay/till unit (Moncur, 2010).

To determine if leakage of weathering products from the till could be responsible for the distributions of U in the porewater and solid phases detailed quantitative mineralogical characterizations were performed to see if U-bearing minerals are present in the sediment. Two types of U-bearing zircons [$ZrSiO_4$] were identified in low abundances in all four samples (Figure 9), and a few rare grains of U-bearing monazite [$(Ce,La,Th)PO_4$] were also identified (Figure 10). Both of these minerals have also been observed in clay tills in Southern Saskatchewan (Yan et al.,2000).

The zircons identified at the Bonnyville sites range from fairly pure end-member ($[Zr,Hf]SiO_4$) which yield good totals (close to 100 wt.%) to zircons with significant amounts of Ca, Fe, and phosphorus (P) and with significantly lower total yields. Although both compositional types of zircon occur as discrete homogeneous grains (Figures 9a and b) they are also observed coexisting as distinct growth zones in a single grain (Figures 9c and d). The UO_2 content of the zircons sampled were significant (average: 1050 ppm) but highly variable ranging from below detection limit of 90 ppm to 4500 ppm. The Ca-, Fe-, and P-bearing zircons were typically the minerals richest in U. Their low totals yields, and the presence of dessication cracks (Figures 9b, c, and d) may be due to partial hydration. Consequently, this type of zircon may well represent replacement of radiation-damaged metamict zircons, also observed by Delattrie et al., 2007, in lateritic soils.

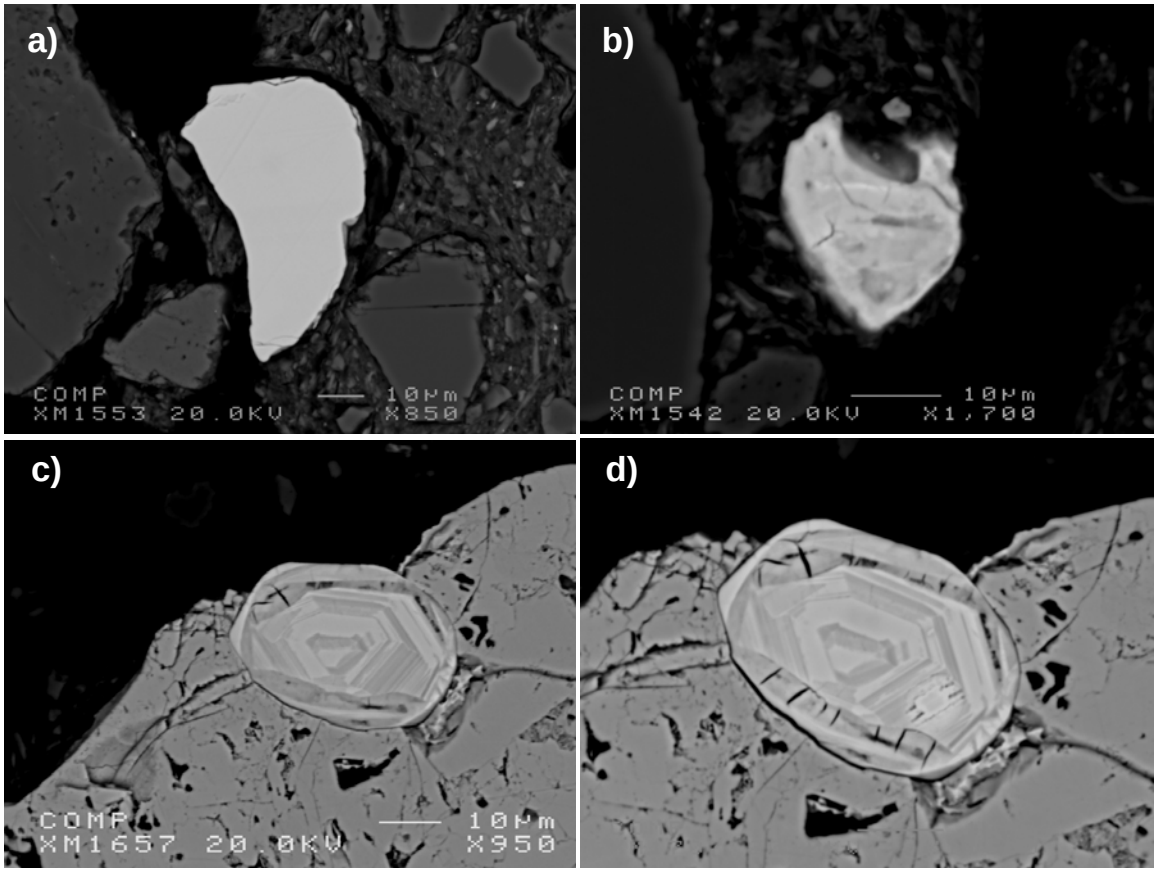

Figure 9: Backscattered electron imaging (BSE) images of sediments showing distinct zircon appearances. a) Near end-member zircon; b) Ca-, Fe-, and P-bearing zircon (note minor desiccation cracks; c) and d) single zircon grain showing coexisting end-member (bright) and Ca-, Fe-, P-bearing growth zones (dark). Note the evolution of desiccation cracks in the dark region (from c to d) after long exposure to the electron beam.

Pure-end member zircons are typically very resistant to weathering and dissolution (Morton and Hallsworth, 1999; Velbel, 1999), and if this was the only type of zircon in the sediments from the Bonnyville sites they would have been an unlikely source of significant U contributions to groundwater. However, the Ca-, Fe-, and P-bearing low-total metamict zircons identified in the sediment not only display weathering features, but also show important similarities to metamict zircons. Metamict zircons can readily alter in near surface environments (Delattrie et al., 2007; Hay and Dempster,2009), and can dissolve at near neutral pH and low temperatures (25 ^{0}C; Tromans, 2006).

The congruent dissolution of zircon results in the release of aqueous species of Zr, silicon (Si) and acid through the following reaction:

$$ZrSiO_4 + 3H_2O \rightarrow H_2SiO_4^{2-} + HZrO_3^{-} + 3H^+ \quad \text{(Equation 12)}$$

and the incongruent dissolution of zircon results in the precipitation of a Zr-oxide through the following (Tromans, 2006):

$$ZrSiO_4 + 2H_2O \rightarrow H_2SiO_4^{2-} + 2H^+ + ZrO_2 \quad \text{(Equation 13)}$$

During the dissolution of zircon in equations 12 and 13, metals such as U, lead (Pb) and rare earth elements (REE) incorporated within the zircon structure can be released to the adjacent pore water. Previous studies have found that the leaching of zircon to be a source of Zr, Pb, and rare earth elements (REE) to groundwater (Stern et al., 1966; Balan et al., 2001; Shand et al., 2005). Therefore metamict zircon potentially represents a major source of U in the groundwater at Sites 1 and 2.

The U-bearing monazite grains (Figure 10) were very rich in UO_2, with abundances ranging from 0.11 to 2.73 wt%, but were rare within the sediment samples.

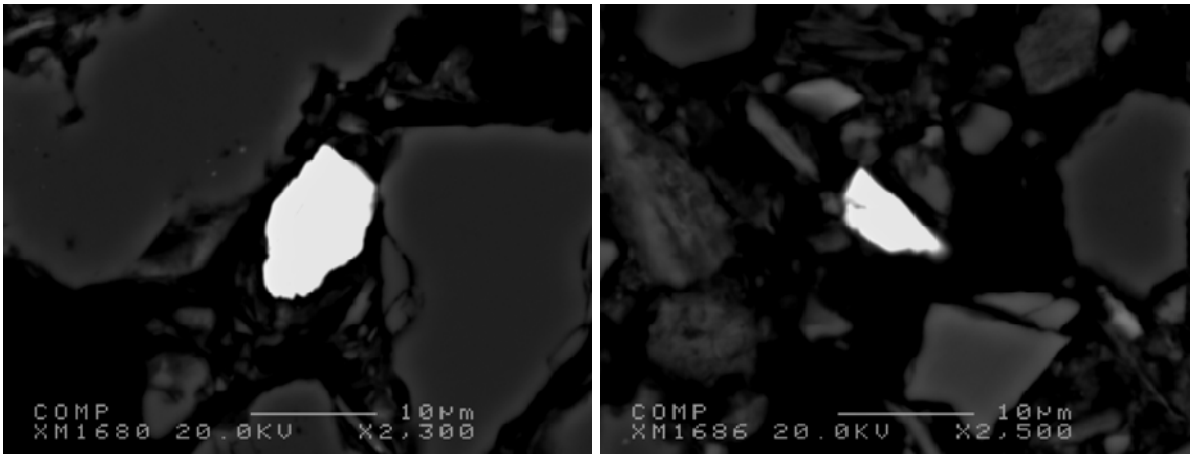

Figure 10: Backscattered electron imaging (BSE) images showing grains of monazite identified in the clay/till at Sites 1 and 2.

Clay minerals are another possible U carrier, however the low bulk U concentration indicates that the levels would be much lower than the levels that can be detected using the WDS-EPMA.

To determine if secondary minerals are controlling U concentrations, saturation indices were calculated using the geochemical model PHREEQC. Calculated SI values for and U(VI) minerals rutherfordine [UO_2CO_3], schoepite [$(UO_2)_8O_2(OH)_{12}\cdot 12(H_2O)$], uranium hydroxide, and Gummite [UO_3] indicate that the pore water from both the Site 1 and Site 2 are undersaturated with respect to these mineral phases (Figures 11 and 12). However, calculated SI values for U(IV) minerals uraninite [UO_2] and amorphous UO_2 and coffinite [$USiO_2$] show that the pore water below the water table at Site 1 is approaching or at saturation with respect to secondary U(IV) mineral phases and may be controlling concentrations of dissolved U(IV). The pore water at Site 2 was undersaturated with respect to all secondary U(IV)mineral phases. In addition, no secondary U mineral phases were in fact observed in the clay/till or aquifer material during mineralogical analysis, possibly due to low concentrations, lower than the levels that can be detected using the WDS-EPMA.

Calculations with PHREEQC show that the pore waters at Site 1 and Site 2 are at equilibrium or supersaturated with Fe-oxyhydroxides, calcite, dolomite and other carbonate minerals, suggesting that these phases may act as possible sinks for dissolved U concentrations. (Figures 11 and 12).

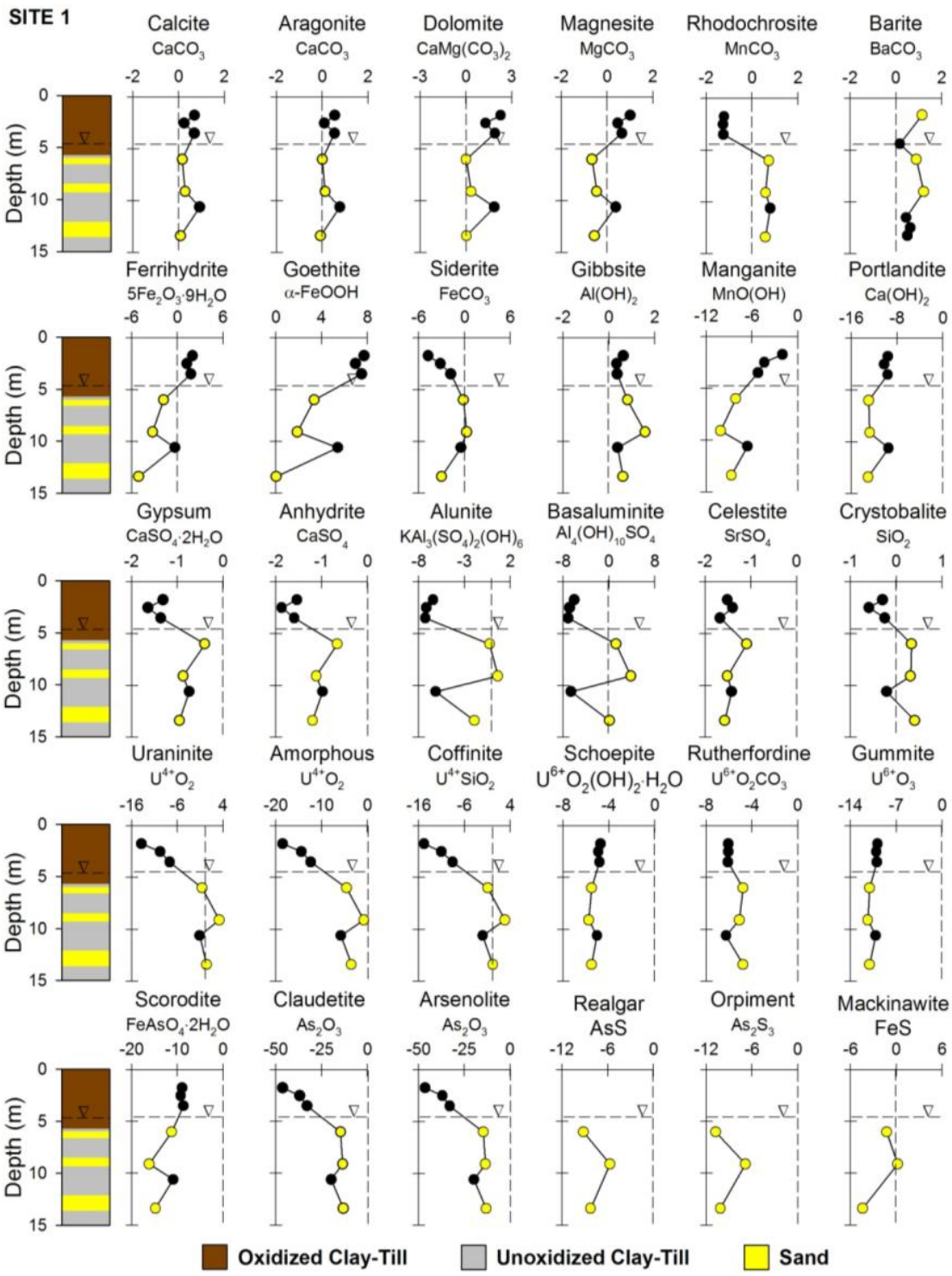

Figure 11: Depth profile from Site 1, MW1, showing stratigraphy and saturation indices calculated using PHREEQC. The horizontal dashed line, with an inverted triangle above, represents the water table and the vertical dashed line represents saturation (zero).

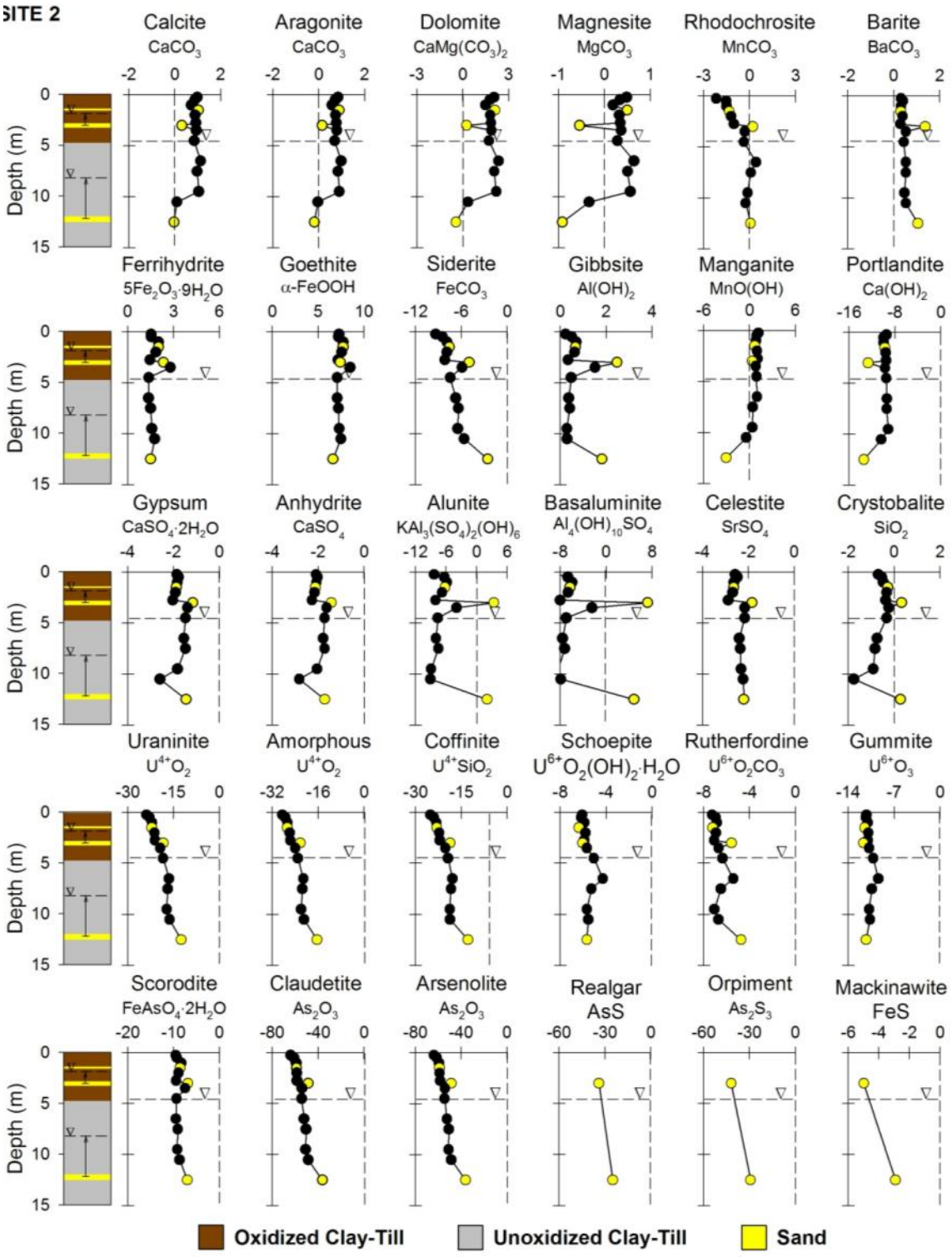

Figure 12: Depth profile from Site 2, MW1, showing stratigraphy and saturation indices calculated using PHREEQC. The horizontal dashed line, with an inverted triangle above, represents the water table and the vertical dashed line represents saturation (zero).

A greenish-white secondary precipitate was collected at Site 1, Well 1, from the plumbing fixtures. Total digestion of the secondary precipitate shows that Ca is the dominate cation

(Table 3) suggesting that the mineral phase could be poorly crystalline secondary carbonate mineral, which is consistent with the carbonate saturation indices calculated in the speciation modeling. Also measured from the total digestion was a significant concentration of U (143 mg/kg), indicating that some U is precipitating or co-precipitating and being removed from solution (Table 3). Elevated copper (Cu) and Zn concentrations could be due to leaching from copper plumbing.

Table 3: Total concentrations extracted from secondary precipitates collected from Site 1 in Well 1 and Well 4.

Location	U (mg/kg)	Ca (mg/kg)	Mg (mg/kg)	Fe (mg/kg)	Cu (mg/kg)	Zn (mg/kg)	Al (mg/kg)	As (mg/kg)	Mn (mg/kg)
Well 1	143	282107	16162	488	19913	3838	183	1.47	328
Well 4	0.59	468	92.9	854	0.44	216	6.32	0.004	2.8

The crystalline phases identified by powder XRD (X-Ray Diffraction Analysis)for the secondary precipitate collected from the surface of plumbing fixture of Well 1,Site 1 consist of monohydrocalcite [$CaCO_3 \cdot H_2O$], aragonite [$CaCO_3$], hydromagnesite [$Mg_5(CO_3)_4(OH)_2 \cdot 4H_2O$], nesquehonite [$Mg(HCO_3)(OH) \cdot 2H_2O$] and gypsum [$CaSO_4 \cdot 2H_2O$]. Because the U content of this sample was fairly high (143 ppm), a more detailed characterization of the main phases was made. Monohydrocalcite appears to be the major phase and typically shows colloform growth sometimes interlayered with denser aragonite. Both phases are fairly close to their Ca end-members and, interestingly contain significant amounts of Cu and Zn likely originating from leaching of copper plumbings (Moncur, 2010) and potentially adsorbed on the carbonates. More porous fragments, dominated by an Mg-rich carbonate were also observed. Micro-XRD analysis of the material indicates that it consists mainly of hydromagnesite roughly intergrown with monohydrocalcite. Finally a small amount of gypsum is present in some of the fragments. Trace element analyses with the EPMA (electron probe micro analyzer) indicated that significant U may have co-precipitated with the Ca-rich carbonates, in particular monohydrocalcite. No significant U was detected in the Mg-carbonate (hydromagnesite).

The U L_{III}-edge XANES spectrum of the secondary precipitates can be used to determine the valence state of the U. The absorption peak (dashed line) is at 17174.4 eV and its derivative is located at 17170 eV. These values suggest that uranium occurs in the U(IV) state. Uranium L_{III}-edge XANES spectrum including its post-edge spectral features (arrow on Figure 13) are similar to the spectra of U(IV) coprecipitated with calcite and aqueous $UO_2(CO_3)_3^{4-}$ (Reeder et al. 2000; 2001) and U^{6+} standards (Michalsen et al. 2006; Regenspurg et al. 2010).

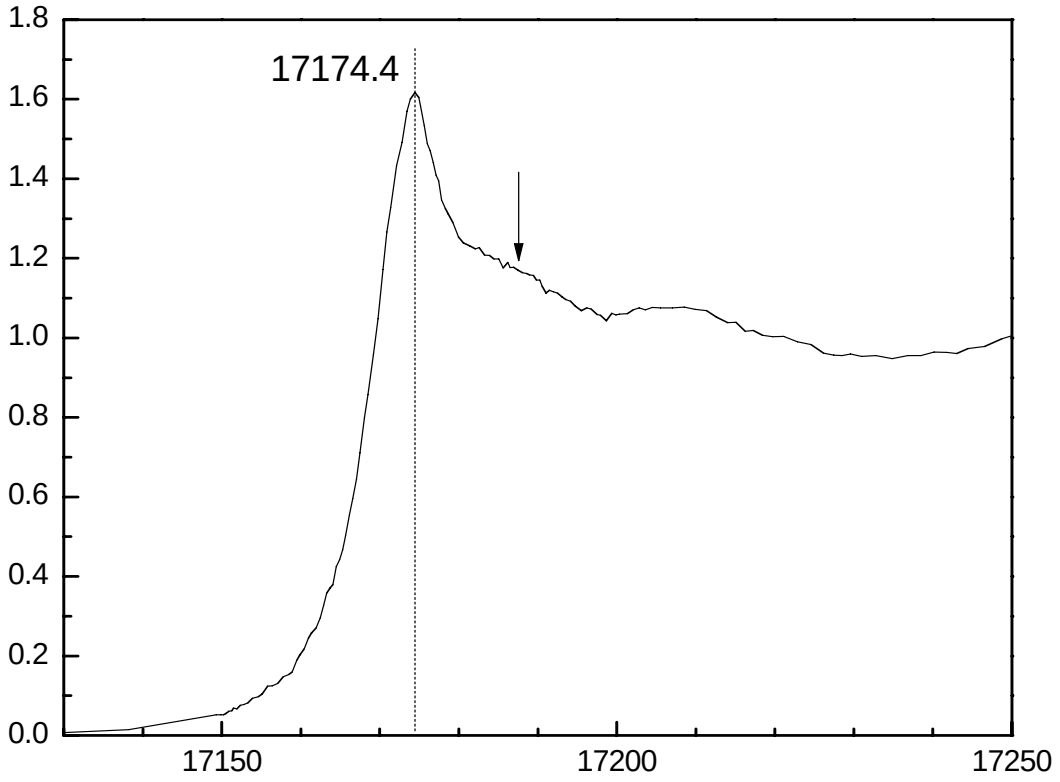

Figure 13. Normalized U L_{III}-edge XANES spectrum of the secondary precipitate collected from Site1, Well 1. The arrow is pointing to a characteristic post-edge feature of U^{6+}.

An orange secondary precipitate was collected from the bottom of Well 4, Site 1. Total digestion of the precipitate indicate that the dominant ion is iron, suggesting that the precipitate is likely a poorly crystalline Fe-oxyhydroxide mineral phase such as goethite (Table 3), which is supported by the saturation indices calculated in the speciation modeling (Moncur, 2010). Observation of the powder XRD pattern indicates that the precipitate consists essentially of goethite [α-FeO(OH)], quartz and calcite. Although U was measureable, concentrations were too low (0.59 mg/kg, Table 3), to use WDS-EPMA and XAFS to further characterize the phases present. However, the presence of U in these secondary precipitates does indicate that some U is being removed from solution possibly by precipitating, co-precipitating or adsorbing to the Fe-oxyhydroxides (Hsi and Langmuir, 1985; Duff and Amrhein, 1996; Logue et al., 2004).

$^{234}U/^{238}U$ Isotpe Ratios

Uranium isotopes, ^{234}U ($t_{1/2,\ U\text{-}234}$=244.5 kyears) and ^{238}U ($t_{1/2,\ U\text{-}238}$= 4,468 Myears), have been used extensively to characterize groundwater systems. There is a fairly large range in $^{234}U/^{238}U$ activity ratios (AR) (e.g. 0.5 to 40, Osmond and Cowart, 1992) making them useful for investigations of groundwater flow, aquifer mixing and tracing anthropogenic sources (Ivanovich et al., 1991; Kronfeld et al., 1994; Toulhoat et al., 1996; Barbieri and Voltaggio, 1998; Eliott et al., 1999; Paces et al, 2002).

The $^{234}U/^{238}U$ isotope ratios were measured in water from the six wells and one clay porewater sample at Site 1, and three wells and four clay porewater samples from Site 2 (Table 4). The

results show minimal variation in the $^{234}U/^{238}U$ isotope ratios between groundwater from the wells and four aquifers, with average $^{234}U/^{238}U$ ratio of 62.07 ppm and standard deviation of only 1.6 ppm.

Table 4: $^{234}U/^{238}U$ isotope ratios in groundwater from Site 1.

Location	Depth (m)	Unit	$^{234}U/^{238}U$ Isotope Ratio (ppm)
Site 1 - C-3.5	3.5	Clay Porewater	59.4
Site 1 - Well1	6.69	Aquifer	61.7
Site 1 - MW2	7.16	Aquifer	63.0
Site 1 - Well 2	7.41 (12.15)	Aquifer	62.4
Site 1 - Well 4	10.14	Aquifer	64.2
Site 1 - Well 3	21.45	Aquifer	61.2
Site 1 - Well 5	24.76	Aquifer	65.5
Site 2 - K1-0.5	0.5	Clay Porewater	60.7
Site 2 - K1-2.75	2.75	Clay Porewater	60.8
Site 2 - K1-3.5	3.5	Clay Porewater	60.9
Site 2 - K1-4.5	4.5	Clay Porewater	61.3
Site 2 - Well1	12.34	Aquifer	62.2
Site 2 - MW1-3	12.49	Aquifer	64.2
Site 2 - Well 3	26.76	Aquifer	61.6

The $^{234}U/^{238}U$ isotope ratio signatures show very little variability between the two sites and over the large range of U concentrations measured (Figure 14). The uniform nature of the $^{234}U/^{238}U$ ratios despite variations in U concentration or depth, provides strong evidence for a single source of U for the groundwater at the site.

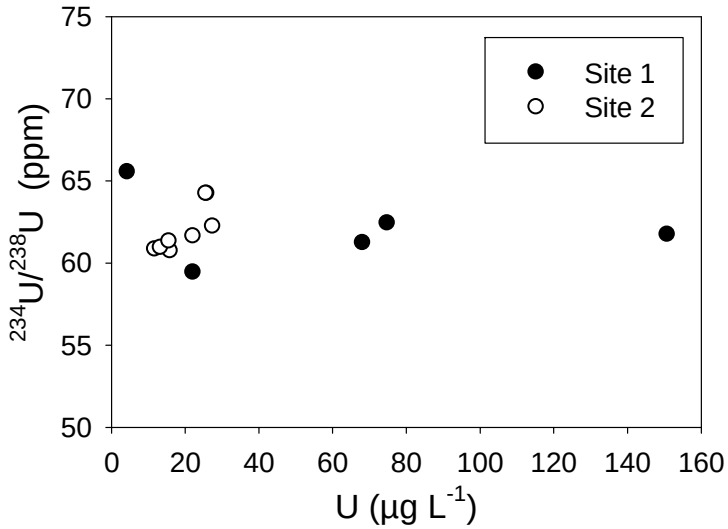

Figure 14. Plot showing dissolved uranium concentrations vs. $^{234}U/^{238}U$ ratios in ppm measured from groundwater in water wells at Site 1 and Site 2.

Arsenic

Dissolved As concentration collected from pore water and groundwater at Site 1, MW1, showed peak concentrations in the clay-till with lower concentrations in the sand units. Arsenic pore water concentrations in the clay averaged 6 µg/L and peaked at 10 µg/L at a depth of 14.5 m (Figure 6). The average dissolved concentration of As in the three saturated sand units was 2.1 µg/L (Table 1).

Pore water collected from the clay-till at Site 2, MW1 had an average dissolved As concentration of 6.9 µg/L, with a peak concentration of 11.7 µg/L at a depth of 9.5 m. (Figure 7). The average concentration of dissolved As in the saturated sand and silt units was 6.1 µg/L, peaking a 8.7 µg/L at a 1 m depth. Overall, the highest concentration of dissolved As are found in the clay-till sediments at Sites 1 and 2.

To determine if leakage of weathering products from the till could be responsible for the distribution of As in porewater and solid phases, detailed quantitative mineralogical characterizations were performed to see if As-bearing minerals are present in the sediment. Small pyrite [FeS_2] grains, typically framboidal in habit (Figures 15a and b) were found throughout the unweathered samples. Since pyrite is a common As carrier (Nordstrom, 2002), a number of BSE (backscattered electron imaging) images of individual grains were taken and their compositions were analyzed by WDS (wavelength dispersive X-ray spectrometry) to determine whether As was a significant compositional component. The As content of pyrite in both samples was variable, reaching 1550 ppm in sample Site 1-6 m and 1840 ppm in sample Site 2-11.5 m, with averages of 460 and 590 ppm respectively. The presence of As in the pyrite grains analyzed suggests that pyrite is the main As carrier in these sediment samples. Pyrite is not stable in aerobic conditions and oxidizes to Fe-oxyhydroxides releasing SO_4 and associated trace metals such as As (Smedley and Kinniburgh, 2002). None of the pyrite grains examined from the unoxidized clay till units showed any evidence oxidation features. The clay-till samples from the oxidized zone (Site 1-1 m, and Site 2-1 m) did not have any framboidal pyrite present, but instead contained spheroidal Fe-oxyhydroxide grains with minor sulpfur (S) and variable trace As (Figure 15 c and d). The habit and composition strongly suggest that these Fe oxyhydroxide grains represent former framboidal pyrite grains. The As content of the characterized Fe-oxyhydroxide reached levels up to 670 ppm in Site 1-1 m and 2270 ppm in Site 2-1 m with averages of 200 and 770 ppm, respectively.

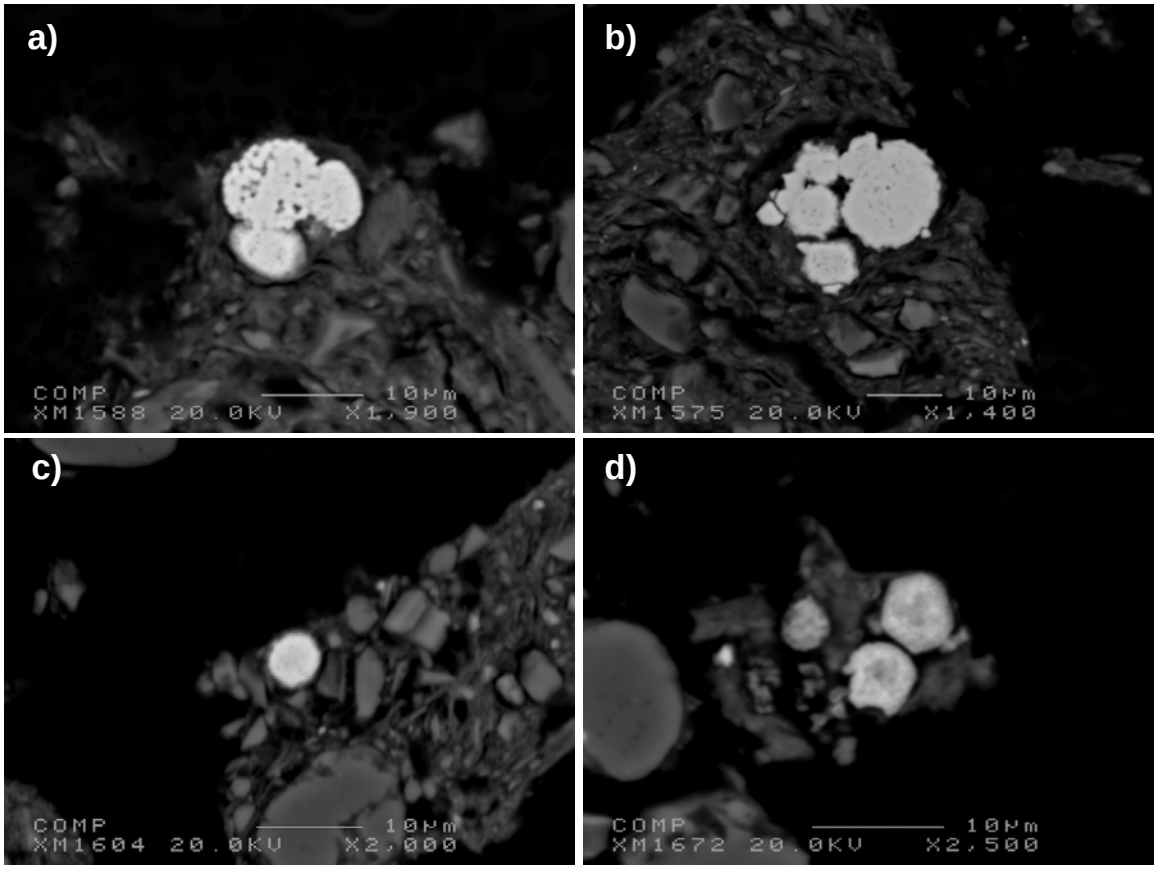

Figure 15: BSE images of representative framboidal grains observed in sediment samples. Framboidal pyrite: Site 1 - 6 m (a), and Site 2 - 11.5 m (b). Framboidal Fe-oxyhydroxide: Site 1 – 1 m (c), and Site 2 – 1 m (d).

The K-edge XANES spectrum was applied to determine the valence state in which arsenic occurs, as described below. Note that As can occur within the structure of arsenopyrite and pyrite as As^{1-}, susceptible to oxidation especially in the framboidal types of pyrite (Paktunc 2008). All of the sediments with elevated levels of As concentrations (4.3 to 7.4 mg/kg) are characterized by the main absorption peak centred at 11874.7 eV (dashed line) indicating that the dominant species are As^{5+}(Figures 16 and 17). The spectral features above the edge in Figures 16 and 17 are similar to those of goethite or ferrihydrite with adsorbed arsenic (Paktunc et al. 2004 and 2008), suggesting that these Fe(III)-oxyhydroxides are the dominant As carriers in the clay-till units with elevated As concentrations. The sediment samples at 5.5 and 6 m depths along bore-hole Site 1- 1 m representing oxidized and unoxidized clay-till display similar XANES spectra dominated by As^{5+}. The oxidized clay and unweathered clay samples from 1 and 11.5 m depths along the Site 2 bore-hole display differences in their As K-edge XANES spectra. The unweathered sample from 11.5 m depth has a shoulder on the lower energy side of the main absorption peak suggesting the presence of reduced arsenic (As^{1-}) species in addition to As^{5+} (Figure 17). The derivative value of this shoulder is 11868.5 eV which is close to those of arsenopyrite and arsenian pyrite suggesting the presence of As^{1-} species in addition to As^{5+}. Preliminary least-squares fitting of the XANES spectra with arsenopyrite and goethite model compounds indicate the proportion of As^{1-} species make up 17 to 26 % of the

total arsenic. The presence of As^{1-} species in the unweathered portions of the clay-till are consistent with the presence of sulfide minerals such as arsenian pyrite and arsenopyrite

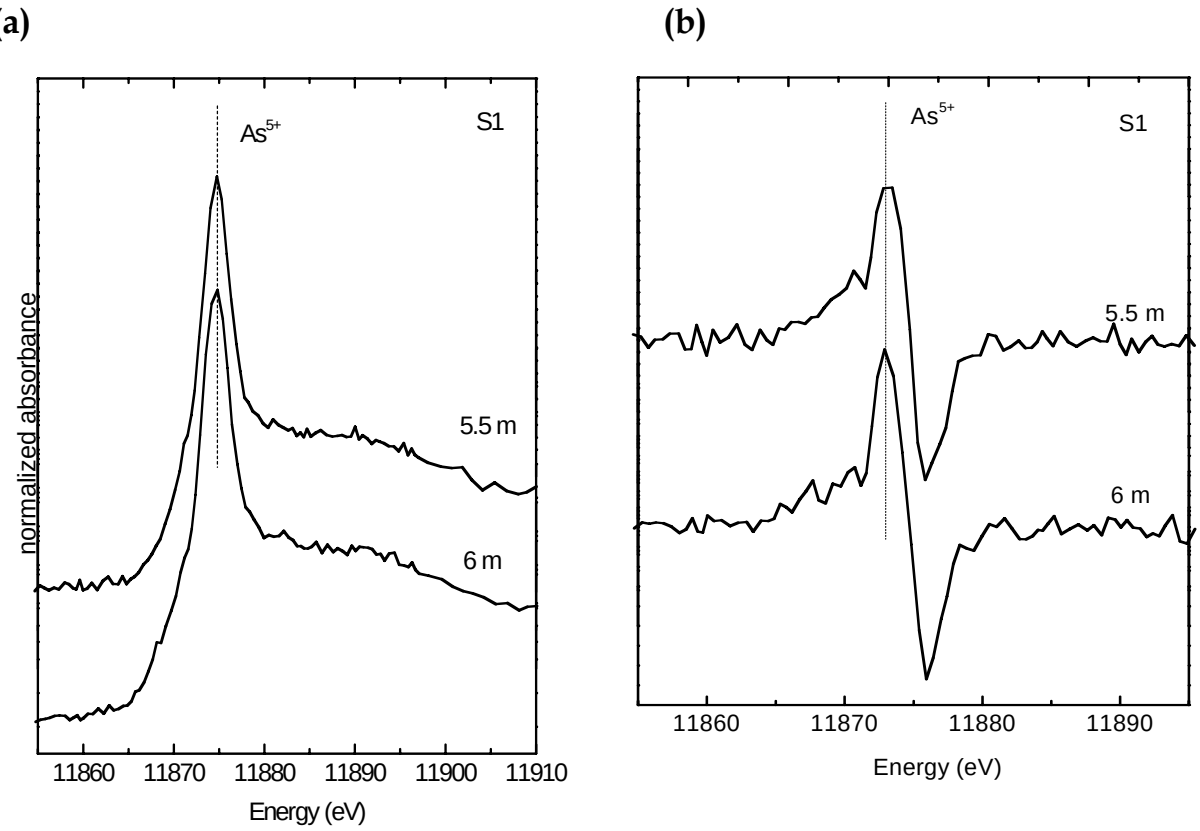

Figure 16. Normalized As K-edge XANES spectra (a) and derivatives (b) of the sediment samples from 5.5 and 6 meter depths from the S1 hole. White line position marked by a vertical dashed line, above, on Figure (a) is at 11874.7 eV.

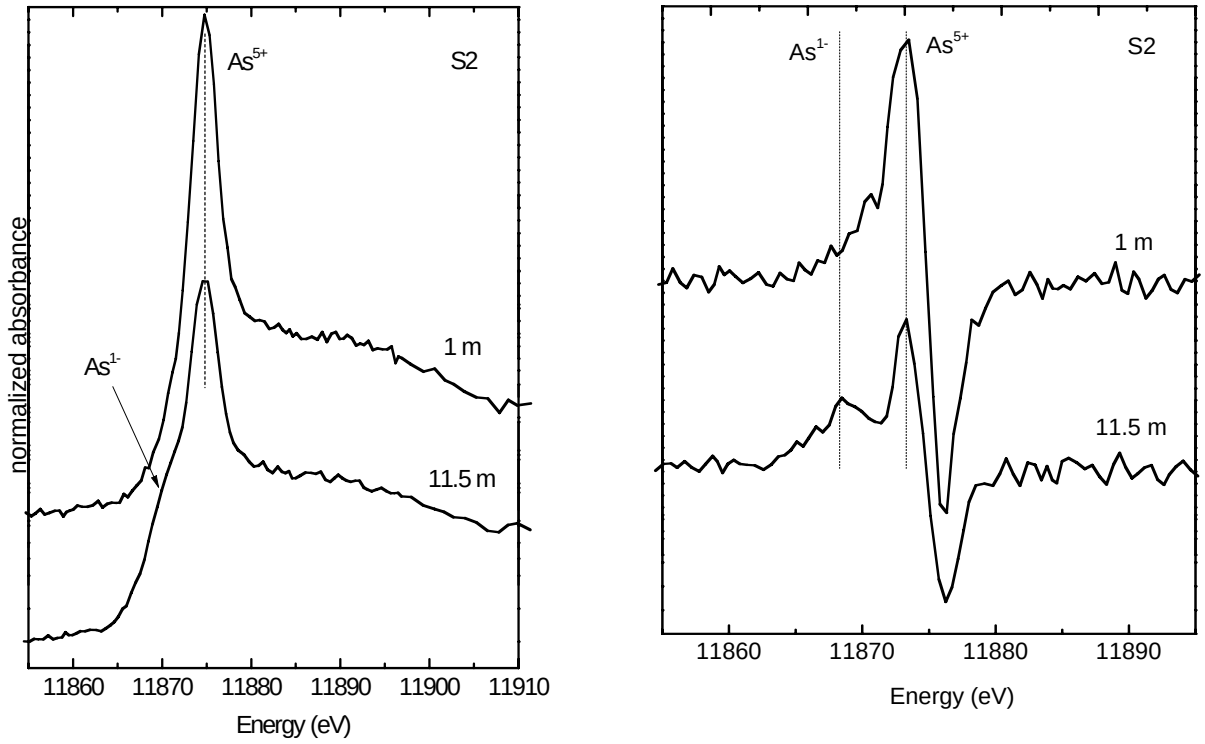

Figure 17. Normalized As K-edge XANES spectra (a) and derivatives (b) of the sediment samples from 1 and 11.5 meter depths from the S2 hole.

The oxidation of arsenian pyrite within the weathered zone can release arsenic to the pore waters, however most of the dissolved As will be removed from solution through co-precipitation with Fe-oxyhydroxides (Smedley and Kinniburg, 2002) and/or adsorption onto Fe-oxyhydroxides (Paktunc et al. 2004; 2008). Below the water table, where groundwater conditions are more reduced, arsenian pyrite and other As-bearing sulfide minerals will be stable and not likely a significant source of As. However, in these reducing settings As may be released during microbial reductive dissolution of Fe-oxyhydroxides:

$$4Fe(OH)_3 + CH_2O + 7H^+ \rightarrow 4Fe^{2+} + HCO_3^+ + 10H_2O \qquad \text{(Equation 14)}$$

During the reduction of Fe-oxyhydroxide by organic carbon [CH_2O] Fe(II), bicarbonate and any other metals absorbed to the Fe-oxyhydroxides such as As will be released to solution. This process is followed by microbially mediated sulfate reduction where sulfate-reducing bacteria catalyze the oxidation of organic carbon reducing SO_4 to hydrogen sulfide (H_2S) (Berner, 1980), through:

$$SO_4^{2-} + 2CH_2O \rightarrow H_2S + 2HCO_3^- \qquad \text{(Equation 15)}$$

The distribution of Fe and SO_4 in porewater at the two sites (Figures 6 and 7) provides support that reductive dissolution of Fe-oxyhydroxides (Equation 14) and sulfate reduction (Equation 15) are occurring. For example, at Site 1, there is an increase of dissolved Fe, general decrease in SO_4 and production of H_2S and reducing conditions.

Speciation modeling from Site 1 shows that the pore water is supersaturated with respect to ferrihydrite (poorly crystalline Fe-oxyhydroxide) within the weathered zone, but is then at saturation or undersaturated below the water table into the reduced zone. Within the weathered zone the oxidation of arsenian pyrite will release arsenic to the pore waters however most of the dissolved As will be scavenged through co-precipitation with Fe-oxyhydroxides (Smedley and Kinniburg, 2002) and/or adsorption onto Fe-oxyhydroxides (Paktunc et al. 2004;2008). The modeling supports the mineralogy results showing that Fe-oxyhydroxides are a potential sink for As in the weathered (oxidized) zone but then through reductive dissolution, they become a potential source of As. Aside from the presence of As bearing Fe-oxyhydroxides, no other secondary As minerals were observed. This finding is also supported by speciation modeling results (Figures 11 and 12).

Conclusions

- Crystalline phases present in the sediments from both Sites 1 and 2 have similar mineralogy composed mainly of quartz, microcline, albite, calcic plagioclase, calcite, amphibole with various amounts of clays minerals. No obvious mineralogical differences are observed between the oxidized and unoxidized till units. The main mineralogical difference between the clay-till and sand sediments are a higher proportion of dolomite and clay minerals in the clay-till

- At Site 1, concentration of dissolved SO_4, major cations and trace metals are elevated in pore water from the near surface weathered till as a result of chemical weathering in the oxidized zone. Lower dissolved ion concentrations observed in the weathered zone at Site 2 may be due to a higher soil water content inhibiting weathering processes.

- Elevated concentrations of dissolved nitrate ($NO_{3)}$ and chlorine (Cl) in the weathered zone at Site 1 could be due to the nitrification of manure-fertilizer applied to the soil.

- Mineralogical investigation of the sediments at Site 1 and 2 revealed the presence of two compositions of U-bearing zircon present throughout the samples; zircon and metamict zircon. A few rare grains of monazite were also identified. Although it is possible that some of the primary mineral phases contain uranium (e.g. clay minerals), the low bulk concentration are at concentrations lower than can be detected using the WDS-EPMA.

- Zircon is the primary U carrier. The observed metamict zircon can readily alter in near-surface environments and displays weathering features. The dissolution of metamict zircon at near neutral pH and low temperature results in the release of aqueous species of Zr, Si and metals such as U, Pb and rare earth elements. Therefore metamict zircon potentially represents a major source of U in the groundwater at Sites 1 and 2.

- The XANES characterization of a U-bearing secondary mineral composed monohydrocalcite, aragonite, hydromagnesite, nesquehonite and gypsum, collected from Well 1, Site 1, indicates that uranium occurs as hexavalent U(U^{+6}). Ca-rich carbonates, in particular Monohydrocalcite, were found to be the main mineral phase to co-precipitate with uranium.

- Elevated concentrations of dissolved U were measured in water bearing silt and sand, and weathered and unweathered clay-till units.

- The $^{234}U/^{238}U$ isotope ratios measured in groundwater from at Sites 1 and 2 show there is minimal variation between sites and groundwater from the wells regardless of U concentration and depth. The $^{234}U/^{238}U$ ratios remain constant, strongly suggesting that the origin of U concentration in the groundwater is from the same source and elevated U concentrations are regional rather a point-source.

- Mineralogical analyses of unweathered clay-till samples reveal the presence of small framboidal pyrite grains throughout samples. Arsenic concentrations in the pyrite reach values of 1550 ppm indicating that pyrite is the main As carrier in the sediment samples.

- No pyrite grains observed show significant oxidation features in the unoxidized clay-till units, however, an examination of clay-till samples form the weathered clay revealed no framboidal pyrite. Instead, the oxidized clay-till samples contained spheroidal Fe-oxyhydroxide grains that contained minor S and variable As, strongly suggesting that these Fe-oxyhydroxide grains represent former framboidal pyrite grains that can easily be oxidized.

- The XANES characterization of sediments from the weathered zone indicates that the primary As species is As^{5+}, supporting that Fe-oxyhydroxides are the dominant As carriers in the clay-till units.

- The XANES characterization of unweathered clay-till samples show the presence of reduced arsenic (As^{1-}) species in addition to As^{5+} indicating that the reduced As is of arsenopyrite and arsenian pyrite. Reduced As species (As^{1-}) make up 17 to 26 % of the total As in the unweathered clay-till.

- Although few elevated concentrations of dissolved As were observed, concentrations were measurable from pore waters throughout the silt, sand and clay-till sediments at both Sites 1 and 2. Dissolved As concentrations were generally higher in the clay-till sediments.

- In the weathered (oxidized) sediments, dissolved As concentrations are likely a result of oxidation reactions whereas in the unweathered (reduced) sediments, As concentrations are mainly due to reductive dissolution of Fe-oxyhydroxides.

Recommendations

- Shallow wells in the area should be sampled for U concentrations and possibly $^{234}U/^{238}U$ isotope ratios.

- It would be beneficial to measure stable isotopes of sulfur ($\delta^{34}S\text{-}SO_4$) from groundwater with elevated As concentrations. Sulfur isotope characteristics would help to determine if dissolved sulfate in the groundwater is a result of sulfide oxidation (pyrite oxidation) or from some other source.

Acknowledgements

Funding for this project was provided by Beaver River Watershed Alliance and Alberta Environment and Water. We thank Brent Welsh, Joe Prusak, Eleanor Kneffel, Breege McKiernan, and Cathie Thompson and for their assistance. The authors express thanks to John Gibson for his constructive review which improved this report. The XAFS experiments were performed at the PNC/XOR beamline, Advanced Photon Source, Argonne National Laboratory which is supported by the US Department of Energy under Contracts W-31-109-Eng-38 (APS) and DE-FG03-97ER45628 (PNC-CAT). The XAFS experiments were also supported by the Natural Sciences and Engineering Research Council of Canada through a MRS (Major Resources Support) grant.

Closure

Alberta Innovates – Technology Futures is pleased to present the findings of this investigation into the source and mobility of uranium and arsenic in groundwater from two sites near Bonnyville, Alberta. We look forward to any comments and discussions.

Sincerely,

Michael Moncur, M.Sc.,
Research Hydrogeologist

References

Alberta Health and Wellness, 2000. Arsenic in groundwater from domestic wells in three areas of northern Alberta. Health Surveillance Report, ISBN (0-7785-0708-4).

Andriashek, L.D. and Fenton, M.M., 1989. Quaternary stratigraphy and surficial geology of the Sand River area 73L. Alberta Research Council, Alberta Geological Survey and Terraine Sciences Department, Edmonton, Alberta. Bulletin No. 57, p. 154.

Andriashek, L.D., 2000. Geochemistry of selected glacial and bedrock geological units, Cold Lake area, Alberta. Alberta Geological Survey, Alberta Utilities Board, Edmonton, Alberta. Earth Sciences Report 2000-10, p. 29.

Atlas of Alberta., 1969. Government of Alberta and University of Alberta. University of Alberta Press in association with University of Toronto Press, p. 158.

Balan, E., Neuville, D.R., Trocellier, P., Fritsch, E., Muller, J.-P., Calas, G., 2001. Metamictization and chemical durability of detrital zircon. Am. Mineral. 86, 1025-1033.

Ball, J.W., Nordstrom, D.K., 1991. User's manual for WATEQ4F with revised thermodynamic data base and test cases for calculating speciation of major, trace and redox elements in natural waters. U.S. Geol. Surv. Open-File Rep. 91–183.

Banfield, J.F., Eggelton, R.A., 1988. Transmission electron microscope study of biotite weathering. Clays Clay Miner. 36, 47-60.

Barbieri, M., Voltaggio, M., 1998. Applications of Sr isotopes and U-series radionuclides to the hydrogeology of Sangemini area (Terni, central Italy). Mineral. Petrograph. Acta 41, 119–126.

Betcher, R.N., Gascoyne, M., Brown, D., 1988. Uranium in groundwaters of southeastern Manitoba, Canada. Can. J. Earth Sci. 25, 2089-2103.

Berner, R.A., 1980. Early Diagenesis: A Theoretical Approach. Princton University Press. Princton, NJ.

Böhlke, K.-J., 2002. Groundwater recharge and agricultural contamination. Hydrogeol. J. 10, 153–179.

Delattre, S., Utsunomiya, S., Ewing, R.C., Boelin, J.-L., Braun, J.-J., Balan, E., Calas, G., 2007. Dissolution of radiation-damaged zircon in lateritic soils. Am. Mineral. 92, 1978-1989.

Desaulniers, D.E., Cherry, J.A. & Fritz, P., 1982. Origin, age, and movement of pore water in clayey Pleistocene deposits in south central Canada. In: Isotopic Studies of Hydrologic Processes. Selected papers from a symposium. North Illinois University Press, USA, 45–55.

Desaulniers, D.E. & Cherry, J.A., 1989. Origin and movement of groundwater and major ions in a thick deposit of Champlain Sea clay near Montreal. Can. Geotech. J. 26, 80–89.

Duff, M.C., Amrhein, C., 1996. Uranium(VI) adsorption on Goethite and soil in carbonate solutions. Soil Sci. Soc. Am. J. 60, 1393–1400.

Eliott, T., Andrews, J.N., Edmunds, W.M., 1999. Hydrochemical trends, paleorecharge and groundwater ages in the fissured Chalk aquifer of the London and Berkshire basins, UK. Appl. Geochem. 14, 333–363.

Fanning, K.A., Pilson, M.E.Q., 1973. Interstitial silica and pH in marine sediments: some effects of sampling procedures. Sci. 173, 1228-1231.

Gilliss, M.L., Al, T.A., Blowes, D.W. and Hall, G.E.M., 2004. Dispersion of metals derived from weathering of mineralization under glacial cover: Tillex Cu-Zn deposit, Matheson , Ontario . Geochem. Explor. Environ. Anal. 4, 291-305.

Hay, D.C., Dempster, T.J., 2009. Zircon alteration, formation and preservation in sandstones. Sediment. 56, 2175-2191

Health Canada, 2010. Guidelines for Canadian drinking water quality-summary table. Accessed March 2011 at www.healthcanada.gc.ca/waterquality.

Hendry, M.J., Cherry, J.A., Wallick, E.I., 1986. Origin and Distribution of Sulfate in a Fractured Till in Southern Alberta, Canada. Water Resour. Res. 22, 45-61.

Hendry, M.J., Wassenaar, L.I., 1999. Implications of the distribution of δD in pore waters for groundwater flow and the timing of geologic events in a thick aquitard system. Water Resour. Res. 35, 1751–1760.

Hendry, M.J., Wassenaar, L.I., 2000. Controls on the distribution of major ions in pore waters of a thick surficial aquitard. Water Resour. Res. 36, 503-513.

Hsi, C.-K.D., Langmuir, D., 1985. Adsorption of uranyl onto ferric oxyhydroxides: application of the surface complexation side-binding model. Geochim. Cosmochim. Acta 49, 1931–1941.

Hussain, N., 1995. Supply rates of natural U-Th series radionuclides from aquifer solids into groundwater. Geophysical Research Letters 22, 1521-1524.

Hydrogeological Consultants Ltd., 2002. M.D. of Bonnyville, Regional Groundwater Assessment. Agriculture and Agri-Food Canada, Prairie Farm Rehabilitation Administration, p. 173.

Hydrogeological Consultants Ltd., 2007. Water Well Investigation, Bonnyville Area, SW 15-061-05 W5M. Report prepared for Canadian Natural Resources Ltd.

Ivanovich, M., Fröhlich, K., Hendry, M.J., 1991. Uranium-series radionuclides in fluids and solids, Milk River aquifer, Alberta, Canada. Appl. Geochem. 6, 405-418.

Kronfeld J., Vogel J. C., Talma, A.S., 1994. A new explanation for extreme $^{234}U/^{238}U$ disequilibria in a dolomitic aquifer. Earth Planet. Sci. Lett. 123, 81–93.

Langmuir, D., 1997. Aqueous Environmental Geochemistry. Prentice Hall, New Jersey, p. 600.

Lemay, T., Parks, K., Andriashek, L.D., Michael, K., Jean, G., Kempin, E., Stewart, S., 2005. Regional groundwater quality appraisal, Cold Lake-Beaver River drainage basin, Alberta; Alberta Energy and Utilities Board, EUB/AGS Special Report 73.

Logue, B.A., Smith, R.W., Westall, J.C., 2004. U(VI) adsorption on natural iron-coated sands: Comparison of approaches for modeling adsorption on heterogeneous environmental materials. Appl. Geochem. 19, 1937–1951.

Malmström, M., Banwart, S., Lewenhagen, L.D., Bruno, J., 1996. The dissolution of biotite and chlorite at 25^{o}C in the near-neutral pH region. J. Contam. Hydrol. 21, 201-213.

Mckay, L.D., Gillham, R.W. & Cherry, J.A. 1993. Field experiments in a fractured clay till 2. Solute and colloid transport. Water Resour. Res. 29, 3879–3890.

McKiernan, B., 2011. Analysis of uranium concentrations and the $^{234}U/^{238}U$ isotope amount ratio in air and water samples. University of Calgary BSc. Thesis. p. 24.

Michalsen, M.M., Goodman, B.A., Kelly, S.D., Kemner, K.M., McKinley, J.P., Stucki, J.W., Istok, J.D., 2006. Uranium and technetium bio-immobilization in intermediate-scale physical models of an in situ bio-barrier. Envir. Sci. Technol. 40, 7048-7053.

Moncur, M.C., Ptacek, C.J., Blowes, D.W., Jambor, J.L., 2005. Release, transport and attenuation of metals from an old tailings impoundment. Appl. Geochem. 20, 639-659.

Moncur, M.C., 2010. Uranium anomalies in shallow groundwater near Bonnyville, Alberta. Water for Life: Knowledge and Research Series, ISBN No. 978-0-7785-9952-4. p. 42.
Morton, A.C., Hallsworth, C.R., 1999. Processes controlling the composition of heavy mineral assemblages in sandstones. Sediment. Geol. 124, 3–29.

Murakami, T., Utsunomiya, S., Yokoyama, T., Kasama, T., 2003. Biotite dissolution processes and mechanisms in the laboratory and in nature: Early stage weathering environments and vermiculitization. Am. Mineral. 88, 377-386.

Nordstrom, D.K., 2002. Worldwide occurrence of arsenic in ground water. Sci. 21, 2143-2145.

Núnez-Delgado, A., Lòpez-Periago, Viqueira, E.D.-F., 2002. Chloride, sodium, potassium and faecal bacteria levels in surface runoff and subsurface percolates from grassland plots amended with cattle slurry. Bioresource Technology 82, 261–271.

Osmond, J.K., Cowart, J. B., 1992. Ground water. In Uranium Series Disequilibrium: Application to Earth, Marine, and Environmental Sciences (eds. M. Ivanovich and R. S. Harmon). Oxford University Press, Oxford, pp. 290–333.

Paces, J.B., Ludwig, K.R., Peterman, Z.E., Neymark, L.A., 2002. $^{234}U/^{238}U$ evidence for local recharge and patterns of groundwater flow in the vicinity of Yucca Mountain, Nevada, USA. Appl. Geochem. 17, 751–779.

Paktunc, D., 2004. A computer program for analysing complex bulk XAFS spectra and for performing significance tests. J. Synchrotron Rad. 11, 295–298.

Paktunc, D. (2008) Speciation of Arsenic in Pyrite by Micro-X-Ray Absorption Fine-Structure Spectroscopy (XAFS). Proc. Ninth International Congress for Applied Mineralogy, Brisbane, QLD, 8 - 10 September 2008. AusIMM.

Paktunc, D., Dutrizac, J. and Gertsman, V. (2008) Synthesis and phase transformations involving scorodite, ferric arsenate and arsenical ferrihydrite: Implications for arsenic mobility. Geochimica et Cosmochimica Acta 72, 2649-2672.

Paktunc, D., Foster, A., Heald, S., and Laflamme, G. (2004) Speciation and characterization of arsenic in gold ores and cyanidation tailings using X-ray absorption spectroscopy. Geochimica et Cosmochimica Acta 68, 969-983.

Parkhurst, D.L., Appelo, C.A.J., 1999. User's guide to PHREEQC (version 2) - a computer program for speciation, batch-reaction, one-dimensional transport, and inverse geochemical calculations. US Geol. Survey, Water-Resour. Inv. Rep. 99-4259, 312 p.

Ranville, J.F., Hendry, M.J., Reszat, T.N., Xie, Q., Honeyman, B.D., 2007. Quantifying uranium complexation by groundwater dissolved organic carbon using asymmetrical flow field-flow fractionation J. Contamin. Hydrol. 91, 233-246.

Ravel, B., Newville, M., 2005. ATHENA, ARTEMIS, HEPHAESTUS: data analysis for X-ray absorption spectroscopy using IFEFFIT. J. Synchrotron Rad. 12, 537-541.

Reeder, R.J., Nugent, M., Tait, C.D., Morris, D.E., Heald, S.M., Beck, K.M., Hess, W.P., Lanzirotti, A., 2001. Coprecipitation of uranium(VI) with calcite: XAFS, micro-XAS and luminescence characterization. Geochim. Cosmochim. Acta 65, 3491-3503.

Reeder, R.J., Nugent, M., Lamble, G.M., Tait, C.D., Morris, D.E, 2000. Uranyl incorporation into calcite and aragonite: XAFS and luminescence studies. Envir. Sci. Technol. 34, 638-644.

Regenspurg, S., Margot-Roquier, C., Harfouche, M., Froidevaux, P., Steinmann, P., Junier, P., Bernier-Latmani, R., 2010. Speciation of naturally-accumulated uranium in an organic-rich soil of an alpine region (Switzerland). Geochim. Cosmochim. Acta 74, 2082-2098.

Shand, P., Johannesson, K.H., Chudaev, O., Chudaeva, V., Edmunds, W.M., 2005. Rare earth element contents of Primorye, Russia: mineral stability and complexation controls, Chapter 7. In: Johannesson, K.H. (ed.), Rare earth elements in groundwater flow systems, 161-186.

Smedley. P.L., Kinniburgh, D.G., 2002. A review of the source, behavior, and distribution of arsenic in natural waters. Appl. Geochem. 17, 517-568.

Stern, T.W., Goldich, S.S., Newell, M.F., 1966. Effects of weathering on the U-Pb ages of zircon from the Morton Gneiss, Minnesota. Earth and Plantary Science Letters 1, 369-371.

Toulhoat, P., Gallien, J.P., Louvat, D., Moulin, V., 1996. Preliminary studies of groundwater flow and migration of uranium isotopes around the Oklo natural reactors (Gabon). J. Contamin. Hydrol. 21, 3–17.

Tromans, D., 2006. Solubility of crystalline and metamict zircon: a thermodynamic analysis. J. Nucl Mater. 357, 221-233.

Velbel, M.A., 1999. Bond strength and the relative weathering rates of simple orthosilicates. Am. J. Sci. 299, 679–696.

White, 2003. Natural weathering rates of silicate minerals. In: Drever, J.I., (Ed.), Surface and ground Water, Weathering, and Soils. In: Holland, H.D., Turekian, K.K., (Eds.), Treatise on Geochemistry, Vol. 5. Elsevier–Pergamon, Oxford, pp. 133–168.

Yan, X.-P., Kerrich, R., Hendry, M.J., 2001. Distribution of the rare earth elements in porewaters from a clay-rich aquitard sequence, Saskatchewan, Canada. Chem. Geol. 176, 151-172